SEDIMENTOLOGY the journal of the International Association of Sedimentologists

Sedimentology (2020) **67**, 649–676 doi: 10.1111/sed.12658

Amplitude, frequency and drivers of Caspian Sea lake-level variations during the Early Pleistocene and their impact on a protected wave-dominated coastline

ELISABETH L. JORISSEN*, HEMMO A. ABELS†, FRANK P. WESSELINGH‡, SERGEI LAZAREV*, VUSALA AGHAYEVA§ and WOUT KRIJGSMAN*

**Faculty of Geosciences, Paleomagnetic Laboratory 'Fort Hoofddijk', Utrecht University, Budapestlaan 17, Utrecht, 3584 CD, The Netherlands (E-mail: e.l.jorissen@uu.nl)*

†Department of Geosciences and Engineering, Delft University of Technology, Stevinweg 1, Delft, 2628 CN, The Netherlands

‡Naturalis Biodiversity Center, P.O.Box 9517, Leiden, 2300 RA, The Netherlands

§Institute of Geography, Azerbaijan National Academy of Science, Huseyn Cavid Avenue 115, Baku, AZ1143, Azerbaijan

Associate Editor – Fabrizio Felletti

ABSTRACT

The Caspian Sea, the largest isolated lake in the world, witnessed drastic lake-level variations during the Quaternary. This restricted basin appears very sensitive to lake-level variations, due to important variations in regional evaporation, precipitation and runoff. The amplitude, frequency and drivers of these lake-level changes are still poorly documented and understood. Studying geological records of the Caspian Sea might be the key to better comprehend the complexity of these oscillations. The Hajigabul section documents sediment deposited on the northern margin of the Kura Basin, a former embayment of the Caspian Sea. The 2035 m thick, well-exposed section was previously dated by magneto-biostratigraphic techniques and provides an excellent record of Early Pleistocene environmental, lake-level and climate changes. Within this succession, the 1050 m thick Apsheronian regional stage, between *ca* 2·1 Ma and 0·85 Ma, represents a particular time interval with 20 regressive sequences documented by sedimentary and palaeontological changes. Sequences are regressing from offshore to coastal, lagoonal or terrestrial settings and are bounded by abrupt flooding events. Sediment reveals a low energy, wave-dominated, reflective beach system. Wave baselines delimiting each facies association appear to be located at shallower bathymetries compared to the open ocean. Water depth estimations of the wave baselines allow reconstruction of a lake-level curve, recording oscillations of *ca* 40 m amplitude. Cyclostratigraphic analyses display lake-level frequency close to 41 kyr, pointing to allogenic forcing, dominated by obliquity cycles and suggesting a direct or indirect link with high-latitude climates and environments. This study provides a detailed lake-level curve for the Early Pleistocene Caspian Sea and constitutes a first step towards a better comprehension of the magnitude, occurrence and forcing mechanisms of Caspian Sea lake-level changes. Facies models developed in this study regarding sedimentary architectures of palaeocoastlines affected by repeated lake-level fluctuations may form good analogues for other (semi-)isolated basins worldwide.

Keywords Flooding surfaces, isolated basin, Milankovitch cycles, Ponto-caspian, regressive sequences, sea-level oscillations, wave-dominated coast.

INTRODUCTION

Sediment deposited in the Caspian Sea forms excellent geological archives to assess the evolution of coastal sedimentary architecture under repeated lake-level oscillations. The Caspian Sea is the largest isolated lake in the world and forms, together with the Black Sea, the final remnants of the once vast Paratethyan domain (Fig. 1A). The Caspian Sea presents several characteristics that benefit preservation of coastal sedimentary successions, which are commonly limited in the open ocean due to strong coastal erosion during lowstands (Catuneanu *et al.*, 2011). With limited tides, wave and wind activity (Hartgerink, 2005; Medvedev *et al.*, 2016), the Caspian Sea offers enhanced preservation potential for coastal deposits. Furthermore, this basin forms an ideal sediment trap, since tectonic subsidence is extremely high in the south of the basin (Nadirov *et al.*, 1997), as well as in the Kura Basin, forming an embayment of the Caspian Sea, corresponding to the foreland basin of both the Greater and Lesser Caucasus (Jackson *et al.*, 2002a; Allen *et al.*, 2003; Fig. 1B). Strong tectonic uplift of the surrounding mountain ranges, associated with dynamic regional climate (Morton *et al.*, 2003), act as the main drivers of sediment supply into the basin (Abreu & Nummedal, 2007).

The water budget of the Caspian Sea shows strong variations through time, since it is highly dependent on regional changes in evaporation, precipitation and runoff (Degens & Paluska, 1979; Kroonenberg *et al.*, 1997; Arpe *et al.*, 2019). As a result, the Caspian Sea witnessed drastic and frequent lake-level changes up to 150 m amplitude over the last millions of years (Kroonenberg *et al.*, 1997; Popov *et al.*, 2006; Yanina, 2014; Krijgsman *et al.*, 2019). The delicate balance between subsidence, sediment supply and water supply in enclosed basins enhances their sensitivity to lake-level and climate changes (Carroll & Bohacs, 1999). Lake-level variations in isolated basins are therefore often of higher order of magnitude and frequency compared to the open ocean (Bohacs *et al.*, 2003). These fluctuations are considered the main forcing mechanism acting on the evolution of coastal sedimentary architecture (Plint & Nummedal, 2000; Posamentier & Morris, 2000). Documenting coastal successions may provide valuable insights into drivers acting on coastal architecture, improving current

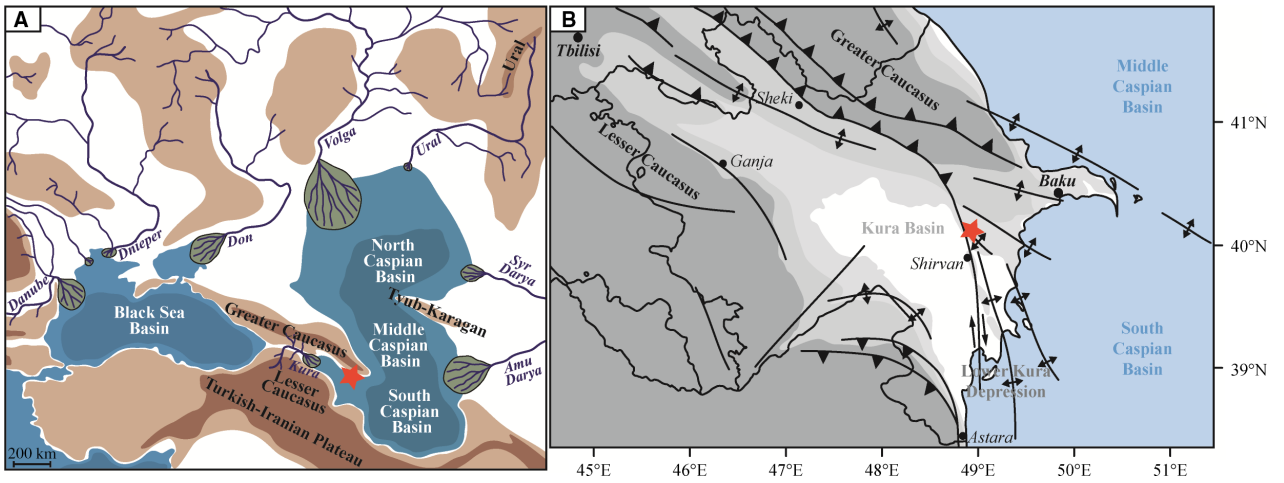

Fig. 1. (A) Palaeogeographical map of the Black Sea and Caspian Sea; the two remnant basins of the ancient Paratethys Sea in the Early Pleistocene with their associated deltas (adapted from Popov *et al.*, 2006, and Abreu & Nummedal, 2007). (B) Structural map of the Kura Basin in light grey, pinched between the Greater and Lesser Caucasus in dark grey (adapted from Jackson *et al.*, 2002a,b). The location of the Hajigabul section is marked by a red star.

understanding of the range, timing and climate forcing of lake-level oscillations in the restricted Caspian Sea.

Lake-level histories have been proposed previously (Jones & Simmons, 1996; Abreu & Nummedal, 2007), yet lack the resolution in the facies and age models to solve driving mechanisms of the Caspian Sea sedimentary evolution. Thick (*ca* 1 km) and continuous (*ca* 1 Myr) sedimentary successions, particularly in the former Kura Basin embayment (Fig. 1B), record frequent relative lake-level variations in the Pleistocene Caspian Sea (van Baak *et al.*, 2013; Forte *et al.*, 2015). Located on the northern margin of the Kura Basin, the Hajigabul section represents a 2 km long, well-dated sedimentary succession that covers much of the Pleistocene (Lazarev *et al.*, 2019). The Early Pleistocene Apsheronian regional stage represents the most dynamic unit along this section, since the Caspian Sea repeatedly engulfed the Kura Basin during this time interval. Apsheronian deposits are marked by frequent alternations between mud-dominated offshore deposits regressing to sand-dominated coastal deposits, and occasionally to mud-dominated pedogenized lagoonal or terrestrial deposits. The remarkable quality of the section, its unique depositional setting and its robust age model are compelling attributes that allowed a detailed reconstruction of Caspian Sea lake-level variations in the Early Pleistocene. The coastal sedimentary architecture of this section is investigated with the intention to provide a detailed record of Caspian Sea lake-level changes. Thanks to the robust age and facies model, the magnitude and frequency of these lake-level variations may be documented throughout the Early Pleistocene. The overall aim is to better understand the drivers of environmental changes in the Caspian Sea, by comparing these oscillations to global climate cycles. This study may lay the foundations to appraise the mechanistic pathways of orbital cycles in restricted basins.

GEOLOGICAL BACKGROUND

Deep marine conditions existed in most of the Caspian Sea until its disconnection from the Black Sea at the end of the Miocene (Popov *et al.*, 2006; Krijgsman *et al.*, 2010). During the Pliocene, the basin was progressively filled in by deltaic sediment of the Productive Series (Reynolds *et al.*, 1998; Hinds *et al.*, 2004), major reservoir rock of the highly productive petroleum system present in the Caspian Sea (Vincent *et al.*, 2010; Abdullayev *et al.*, 2012). The basin underwent a major transgression following a likely Arctic flooding event during the Late Pliocene/Early Pleistocene Akchagylian regional stage (Richards *et al.*, 2018; van Baak *et al.*, 2019). The Caspian Sea became fully isolated from marine conditions around 2·5 Ma (Richards *et al.*, 2018). The Quaternary succession is consequently subdivided into regional chronostratigraphic units (see Krijgsman *et al.*, 2019, for details) (Fig. 2A). During the Early, Middle and Late Pleistocene Apsheronian, Bakunian, Khazarian and Khvalynian regional stages, the Caspian Sea experienced strong lake-level oscillations and during extreme highstands episodic overflow events occurred towards the Black Sea (Yanina, 2014).

The Caspian Sea is subdivided into a North, Middle and South Basin (Fig. 1A). The South Caspian Basin presents a western extension, known as the Kura Basin, that corresponds to the foreland basin of both the Greater and Lesser Caucasus (Jackson *et al.*, 2002a; Allen *et al.*, 2003; Fig. 1B). Tectonic deformations affected the study area during the Quaternary, creating numerous strike slip faults and folds with mean directions between N130° and N160°. The Hajigabul Anticline, also known as the Hajigabul Mountain, the Kichik Kharami ridge or the Maliy Kharami fold, is located in the northern margin of the Kura Basin. This asymmetrical anticline is approximately 12 km long, 10 km wide and is oriented along a mean direction of *ca* N135° (Fig. 2B). The northern flank, dipping on average 20° to the north, is thrusted on top of the southern flank, dipping on average 65° to the south. The eroded southern flank of the anticline exposes the 2035 m thick Hajigabul section (N40·13640556°, E48·88694444° up to N40·12366389°, E48·86972222°) (Fig. 2C, Appendix S1). The anticline exposes clastic sedimentary deposits dated from the Pliocene Productive Series up to the Middle Pleistocene Khazarian regional stage (Bairamov *et al.*, 2008; Lazarev *et al.*, 2019).

MATERIAL AND METHODS

This study focuses on the repeated lake-level variations during the Early Pleistocene Apsheronian regional stage. Lake-level oscillations were reconstructed based on a detailed sedimentary

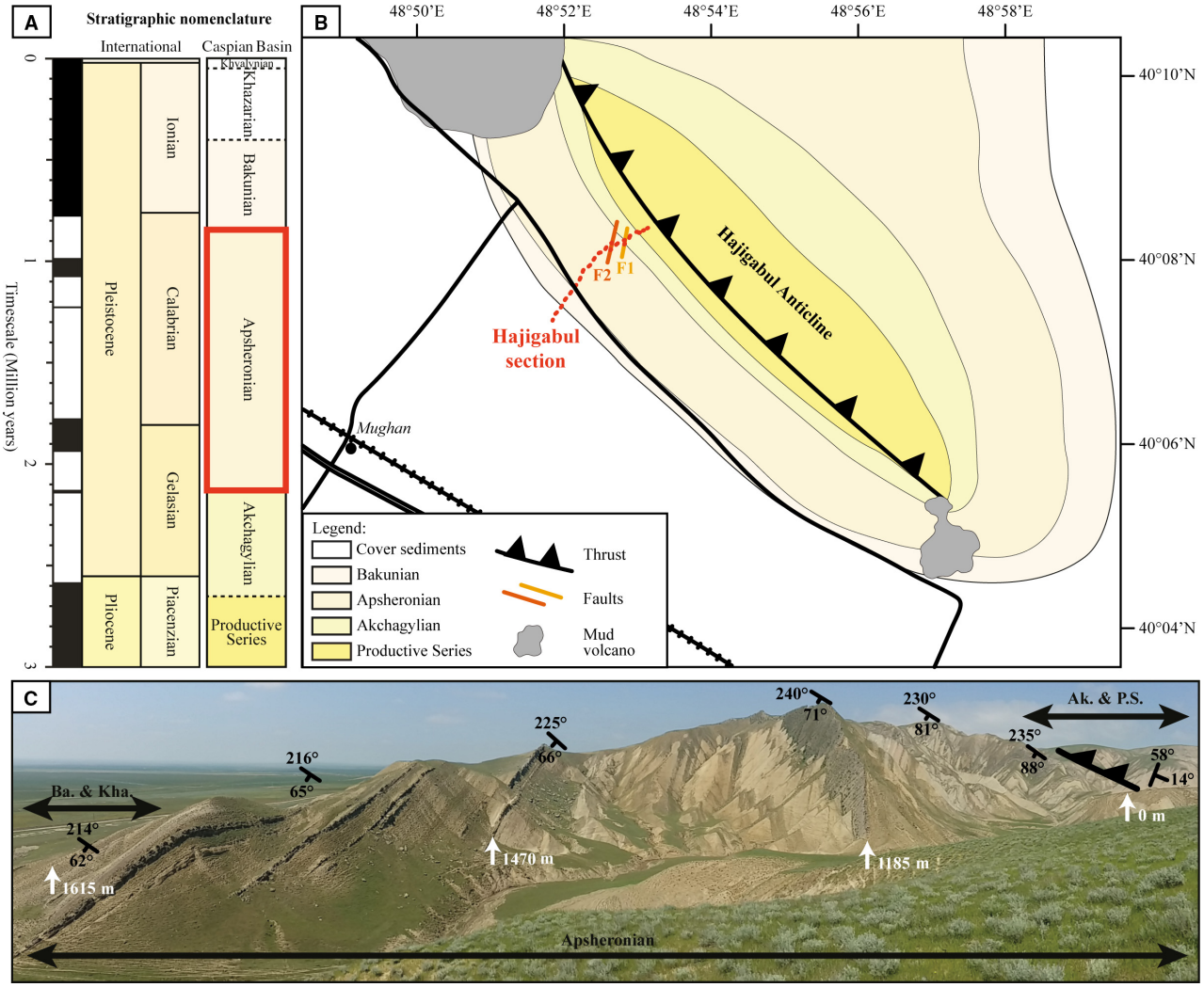

Fig. 2. Stratigraphic context of the Hajigabul Section. (A) Stratigraphic chart of the Productive Series (P.S.), Akchagylian, Apsheronian, Bakunian, Khazarian and Khvalynian regional stages (adapted from Krijgsman *et al.*, 2019). (B) Geological map of the Hajigabul Anticline (adapted from Bairamov *et al.*, 2008). Red line indicates the studied section running along two strike-slip faults F1 and F2. (C) Panorama picture (looking north-west) of the Hajigabul section cropping out along the southern flank of the asymmetrical anticline with some anchor points along the stratigraphy.

log realized along the Hajigabul section at a decimetre-scale. Field observations focused on variations in lithologies, stacking patterns, colours, sedimentary structures and grain-size distributions, as well as the mineralogy, sorting, rounding, sphericity, texture and maturity of the sediment grains. Sediment colours were determined on fresh rocks using Munsell Soil Color Charts. Diverse sedimentary structures were documented, such as graded bedding, lamination, cross-stratification, pedogenic features, convolute bedding and erosional surface. Distinction was made between well-defined lamina, lamination and bed (Campbell, 1967). Petrographic optical microscopic descriptions were performed on 30 μm thick thin-sections, made perpendicular to the progradation direction of the observed sedimentary structures. Palaeocurrent directions were measured on three-dimensional cross-beds and corrected by unfolding the bedding planes. Measurements were subsequently statistically distributed over 12 intervals of 30° and plotted in a rose diagram with a maximum representability of 50%. Sedimentary facies were compared to well-established classifications (Postma, 1990; Miall, 2006), as well as several detailed referenced studies (see *Depositional environments* section). Taphonomic and mollusc

Table 1. Methodology used to identify rhythmic sedimentary variations along the Hajigabul section based on a facies association depth ranking scale.

Facies association depth ranking scale			
Environment	Dominant lithology	Characteristic features	Index
Terrestrial	Mudstone	Pedogenesis, reddish oxidation, freshwater shells	VII
Lagoon	Mudstone	Organic material fragments, freshwater shells	VI
Backshore	Fine to very coarse-grained sandstone	Conglomeratic layers, oligohaline shell pavements	V
Foreshore	Fine to coarse-grained sandstone	Cross-stratification, oligohaline shell strings	IV
Upper shoreface	Mudstone and very fine to medium-grained sandstone	Cross-stratification, lower mesohaline/ oligohaline shell strings	III
Lower shoreface	Mudstone and siltstone	Horizontal lamination, mesohaline/ oligohaline shell strings	II
Offshore	Mudstone	Horizontal lamination, mesohaline/ oligohaline dispersed shells	I

observations provided additional information such as depositional energy, water depth and salinity, supporting environmental reconstructions. Molluscs were defined as *in situ* when presenting paired valves, or as reworked when displaying solitary, fragmented and/or abraded valves. Faunal assemblages are mostly composed of endemic species, identified following regional taxonomies (Andrusov, 1923; Kolesnikov, 1950; Wesselingh *et al.*, 2019). Biotas displayed preferred salinity ranging from freshwater (0 to 0·5 g l^{-1}), oligohaline (0·5 to 5 g l^{-1}) to mesohaline (5 to 18 g l^{-1}) conditions. Integration of data sets permitted to distinguish several facies fashioned by different depositional processes. Related facies were grouped into facies associations, representing distinct depositional environments.

Rhythmic sedimentary patterns between distal clay-dominated and proximal sand-dominated facies associations were assessed along the Hajigabul section. A facies depth rank curve was created ranging from 'I' for the deepest deposits, up to 'VII' for the shallowest deposits (Table 1). The facies depth rank shaped a relative lake-level curve, which was used to identify stratigraphic sequences. Cyclostratigraphical analyses were subsequently realized on the facies depth rank curve. Using standard settings, Blackman-Tukey power spectra were generated with a Bartlett window in the Analyseries 2.0.4b program. Data were normalized to the unit variance and equally-spaced through linear interpolation. In the same program, bandpass filters were applied at 90% confidence levels. The six anchor points of the magnetostratigraphic time frame previously established along the Hajigabul section (Lazarev *et al.*, 2019; Fig. 3A) allowed correlation to the geomagnetic polarity timescale (Gradstein *et al.*, 2012). Based on this age model, cyclostratigraphical analyses allowed estimation of the frequency and timing of the rhythmic environmental changes and evaluation of the potential impact of Milankovitch eccentricity, obliquity and precession astronomical cycles (Laskar *et al.*, 2011) and global sea-level variations (de Boer *et al.*, 2014).

RESULTS

Depositional environments

A depositional model was created along the detailed lithological log of the Hajigabul section (Fig. 3B, Appendix S2). Eight facies associations were assembled representing distal shallow marine to proximal coastal, lagoonal or terrestrial depositional environments (Table 2). Facies associations were defined as sedimentary intervals developing between wave baselines, tide levels or storm levels. However, in the absence of major wave or tide activity in isolated basins, these boundaries were adjusted compared to those established in the open ocean. The

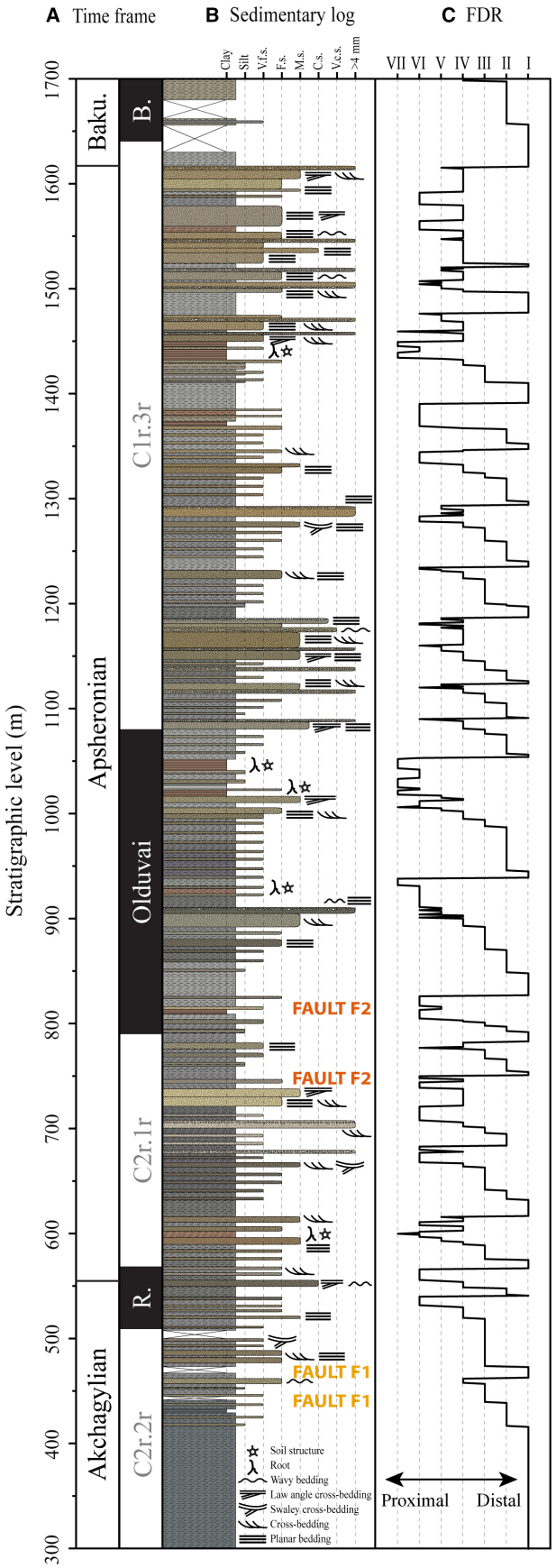

Fig. 3. Hajigabul section, sedimentary log, facies depth rank and age dating results. (A) Magnetostratigraphy and interpreted regional units (Lazarev *et al.*, 2019). (B) Sedimentary log of the Apsheronian interval. The section was continuously logged between two strike-slip faults F1 and F2 with a minor effect on the sedimentary succession. (C) Facies depth rank (FDR) established based on the sedimentary facies associations observed along the section (see Table 1).

storm-wave base (SWB) at the offshore – lower shoreface transition, the fair-weather wave base (FWB) at the lower – upper shoreface transition and the highest storm level at the backshore – continental transition can still be preserved. On the other hand, the mean low tide level at the upper shoreface – foreshore transition and the mean high tide level at the foreshore – backshore transition as found in the open ocean are absent in the Caspian Sea, recording a micro-tidal regime. In this peculiar setting, a classification based on the mean low water level and mean high water level was preferred for the most proximal facies associations, solely dependent on seasonal variations in evaporation, precipitation and runoff.

Offshore facies association (FA.I)

Description

Facies Association I is composed of 1 to 22 m thick dark bluish-grey (GLEY2-4/5B) to dark greenish-grey (GLEY1-4/5G) mudstone. The base of the succession consists of 1 to 10 m thick homogeneous intervals of massive mudstone (Facies Fm). Massive mudstone is overlain by 3 to 15 m thick intervals of mudstone with horizontal planar silt lamination (Facies Fl – Fig. 4A). Lamina sets are 0·5 to 1·0 cm thick and comprise laminae 1 to 3 mm thick. Throughout FA.I, sediment is commonly affected by dispersed low intensity bioturbation, made of 1 to 3 cm long and 0·3 to 0·5 cm wide vertical burrows. Sediment contains some dispersed *in situ* mesohaline to oligohaline mollusc species of *Dreissena*, *Apsheronia*, *Monodacna* and *Hyrcania* (Appendix S3).

Interpretation

Facies Association I documents alternations between very low and low depositional energies. Massive mudstone (Facies Fm) is deposited out of suspension in low energy open waters. Such deposits have previously been identified as hemipelagic deposits (Stow & Tabrez, 1998). Laminated mudstone (Facies Fl) represents intermittent low energy distal bottom-current

Table 2. Lithofacies descriptions and associated processes interpretations. Lithofacies are based on field observations focusing on variations in grain-sizes, ranging from mudstone (mst), silt, very fine sandstone (v.f.sst), fine sandstone (f.sst), medium sandstone (m.sst), coarse sandstone (c.sst) up to very coarse sandstone (v.c.sst), as well as variations in bedding, colours, sedimentary structures, fauna taphonomy and fauna assemblages. F.A. = facies association.

Facies	Lithology	Sedimentary structures	Outcrop exposure	Appearance in outcrop	Mechanism of formation	Process interpretation	F.A.
Muddy shell lag (TS3)	Olive-grey to reddish-brown mst	Erosive base, abundant centimetre-scale clay pebbles, abundant reworked freshwater to oligohaline shells	0·05 to 0·1 m	Slope-forming unit, often scree-covered, laterally continuous	Lag formed under wave reworking	Very high energy flow during flooding event	VIII
Shelly mst. (TS2)	Bluish-grey to greenish-grey mst	Abundant *in situ* and reworked freshwater to oligohaline shells	0·05 to 0·5 m	Slope-forming unit, often scree-covered, laterally continuous	Deposition from suspension	Low energy flow during flooding event	VIII
Conglomeratic shell lag (TS1)	Yellowish-brown m.sst. to v.c.sst	Abundant *in situ* and reworked freshwater to oligohaline shells	0·05 to 0·2 m	Crest-forming unit, extremely resistant beds, laterally continuous	Lag formed under wave reworking	Very high energy flow during flooding event, post-diagenetic induration	VIII
Pedogenized laminated mst. (Pl)	Reddish-brown greenish-grey mst	Horizontal 1 to 3 mm planar lamination of silts and v.f.sst. (sets of 0·5 to 1·0 cm), abundant millimetre-scale organic material fragments, common slickenslides, common roots, common bioturbation, rare *in situ* freshwater shells	1·0 to 5·0 m	Slope-forming unit, often scree-covered, laterally discontinuous	Deposition from suspension alternating with overbank deposition	Low energy standing water with intermittent moderate energy wash-over fans, post-diagenetic pedogenic alterations	VII
Pedogenized massive mst. (Pm)	Reddish-brown to greenish-grey mst	Structureless, abundant millimetre-scale organic material fragments, common slickenslides, common roots, common bioturbation, rare *in situ* freshwater shells	1·0 to 5·0 m	Slope-forming unit, often scree-covered, laterally discontinuous	Deposition from suspension	Low energy standing water, post-diagenetic pedogenic alterations	VII

Table 2. (continued)

Facies	Lithology	Sedimentary structures	Outcrop exposure	Appearance in outcrop	Mechanism of formation	Process interpretation	F.A.
Organic-rich laminated sst. (Cs)	Yellowish-brown v.f.sst to m.sst	Horizontal 1 to 3 mm planar lamination of silts (sets of 0·01 to 0·1 cm), abundant millimetre-scale organic material fragments, rare reworked freshwater to oligohaline shells	0·5 to 5·0 m	Hill-forming unit, resistant beds, laterally discontinuous	Plane-bed flow regime under sediment traction	High energy overbank deposition during wash-over fans	VI
Organic-rich laminated mst. (Cl)	Olive-grey to reddish-brown mst	Horizontal 1 to 3 mm planar lamination of silts (sets of 0·5 to 3·0 cm), abundant millimetre to centimetre-scale organic material fragments, common roots, rare bioturbation, rare charophytes, rare fish bones, common *in situ* freshwater to oligohaline shells	1·0 to 15·0 m	Slope-forming unit, often scree-covered, laterally discontinuous	Deposition from suspension alternating with overbank deposition	Low energy standing water with intermittent moderate energy wash-over fans	VI
Organic-rich massive mst. (Cm)	Olive-grey to reddish-brown mst	Structureless, abundant millimetre to centimetre-scale organic material fragments, common roots, rare bioturbation, rare charophytes, rare fish bones, common *in situ* freshwater to oligohaline shells	1·0 to 5·0 m	Slope-forming unit, often scree-covered, laterally discontinuous	Deposition from suspension	Low energy standing water	VI
Conglomeratic sst. (Gm)	Yellowish-brown f.sst. to v.c.sst	Clast-supported conglomeratic sst., common centimetre-scale lithic pebbles, common centimetre-scale mud clasts, common centimetre-scale organic material fragments, abundant reworked oligohaline shells, common induration	0·1 to 0·5 m	Crest-forming unit, extremely resistant beds, laterally continuous	Lag formed under wave reworking	Very high energy flow in the swash zone, post-diagenetic induration	VI
Low-angle cross-laminated sst. (Sa)	Yellowish-brown f.sst. to c.sst	Low-angle cross-lamination (sets of 5 to 50 cm), common reworked oligohaline shells	0·5 to 5·0 m	Crest-forming unit, extremely resistant beds, laterally continuous	Migration of low relief dunes under swash and backwash currents	High energy half-stationary wave oscillation in close touch with sediment floor	V

Table 2. (continued)

Facies	Lithology	Sedimentary structures	Outcrop exposure	Appearance in outcrop	Mechanism of formation	Process interpretation	F.A.
Wavy-bedded sst. (Sw)	Yellowish-brown f.sst. to c.sst	Symmetrical current ripple cross-lamination (sets of 5 to 50 cm), amplitude of 3 to 5 cm and wavelength of 7 to 10 cm, common reworked oligohaline shells	0·5 to 3·0 m	Crest-forming unit, extremely resistant beds, laterally discontinuous	Migration of 2D straight-crested dunes	High energy stationary wave oscillation in close touch with sediment floor	V
Swaley cross-stratified sst. (Ss)	Greyish-brown f.sst. to m.sst	Swaley cross-stratification (sets of 5 to 50 cm), common normal grading, common sediment loading, common reworked oligohaline shells	0·5 to 3·0 m	Hill-forming unit, resistant beds, laterally continuous	Migration of 3D straight-crested dunes	Moderate energy bottom-currents	IV, V
Laminated sst. (Sl)	Greyish-brown very f.sst. to v.c.sst	Horizontal 1 to 3 mm planar lamination (sets of 0·01 to 0·1 cm), common normal grading, common sediment loading, common reworked oligohaline shells	0·5 to 8·0 m	Hill-forming unit, resistant beds, laterally continuous	Plane-bed flow regime under sediment traction	High energy bottom-currents	III, IV, V
Cross-stratified sst. (Sc)	Greyish-brown f.sst. to m.sst	Tabular and sigmoidal cross-stratification (sets of 5 to 50 cm), common normal grading, common sediment loading, common reworked oligohaline shells	0·5 to 3·0 m	Hill-forming unit, resistant beds, laterally continuous	Migration of 2D straight crested dunes	Moderate energy bottom-currents	III, IV, V
Trough cross-stratified sst. (St)	Greyish-brown v.f.sst. to m.sst	Trough cross-stratification (sets of 5 to 50 cm), common normal grading, common sediment loading, common reworked oligohaline shells	0·5 to 3·0 m	Hill-forming unit, resistant beds, laterally continuous	Migration of 2D/3D sinuous crested dunes	Moderate energy bottom-currents	III, IV
Lenticular bedded mst. (Fs)	Bluish-grey to greenish-grey mst	Lenticular bedding of silts and f.sst. (sets of 1 to 5 cm), rare bioturbation, rare *in situ* and reworked oligohaline to mesohaline shells	3·0 to 10·0 m	Slope-forming unit, often scree-covered, laterally discontinuous	Deposition from suspension alternating with bottom-currents	Very low energy hemipelagic processes with intermittent moderate wave action	II, III

Table 2. (continued)

Facies	Lithology	Sedimentary structures	Outcrop exposure	Appearance in outcrop	Mechanism of formation	Process interpretation	F.A.
Laminated mst. (Fl)	Bluish-grey to greenish-grey mst	Horizontal 1 to 10 mm planar lamination of silts and f.sst. (sets of 0·5 to 5·0 cm), rare bioturbation, rare *in situ* and reworked oligohaline to mesohaline shells	3·0 to 42·0 m	Slope-forming unit, often scree-covered, laterally continuous	Deposition from suspension alternating with bottom-currents	Very low energy hemipelagic processes with intermittent low to moderate energy density currents	I, II, III
Massive mst. (Fm)	Bluish-grey to greenish-grey mst	Structureless, common bioturbation, common *in situ* oligohaline to mesohaline shells	1·0 to 10·0 m	Slope-forming unit, often scree-covered, laterally continuous	Deposition from suspension	Very low energy hemipelagic processes	I

activities. Similar bottom-currents have been documented as storm-generated currents transporting coastal sediment towards more distal settings (Héquette & Hill, 1993). FA.I represents interchanges between very low and low depositional energies, which are increasing towards the top as lamina sets become thicker and more frequent. Together with the vertical burrows, they point towards depositional environments located in the sublittoral zone. FA.I represents relatively shallow offshore settings, with sediment deposited below the SWB.

Lower shoreface facies association (FA.II)

Description

Facies Association II consists of 2 to 42 m thick dark greenish-grey (GLEY1-4/5G) mudstone. At the base, mudstone contains thicker and coarser-grained horizontal planar lamination of silts to fine sands (Facies Fl). Lamina sets are 1 to 5 cm thick and contain 3 to 10 mm thick laminae. Upward, mudstone displays lenticular bedding made of 1 to 5 cm thick and 3 to 10 cm long asymmetrical lenses composed of silt to very fine sands (Facies Fs – Fig. 4B). Mudstone sporadically alternates with 0·5 to 3·0 m thick beds of greyish-brown (2·5Y-5/2) very fine to medium-grained sandstone. Sandstone is commonly deposited in normal graded beds and comprises three different types of sedimentary structures. Sandstone contains trough cross-stratification filled in with mud, with preserved cross-set thicknesses between 5 cm and 50 cm (Facies St) and presents tabular and sigmoidal cross-stratification, with preserved cross-set thicknesses between 5 cm and 50 cm (Facies Sc). Finally, sandstone comprises horizontal planar lamination (Facies Sl), made of 1 to 10 mm thick lamina sets containing 1 to 3 mm thick laminae. Throughout FA.II, sandstone beds commonly display sediment loading. Sediment documents dispersed low intensity bioturbation made of 1 to 3 cm long and 0·3 to 0·5 cm wide vertical burrows. Sediment also contains rare dispersed *in situ* molluscs, as well as some 1 to 5 mm thick shell strings with transported shells and shell debris, ranging from mesohaline to oligohaline salinities. Observed fauna were *Dreissena*, *Apsheronia*, *Monodacna*, *Hyrcania* and *Clessiniola* species (Appendix S3).

Interpretation

Facies Association II records interchanges between low and moderate depositional energies. Laminated mudstone (Facies Fl) represent

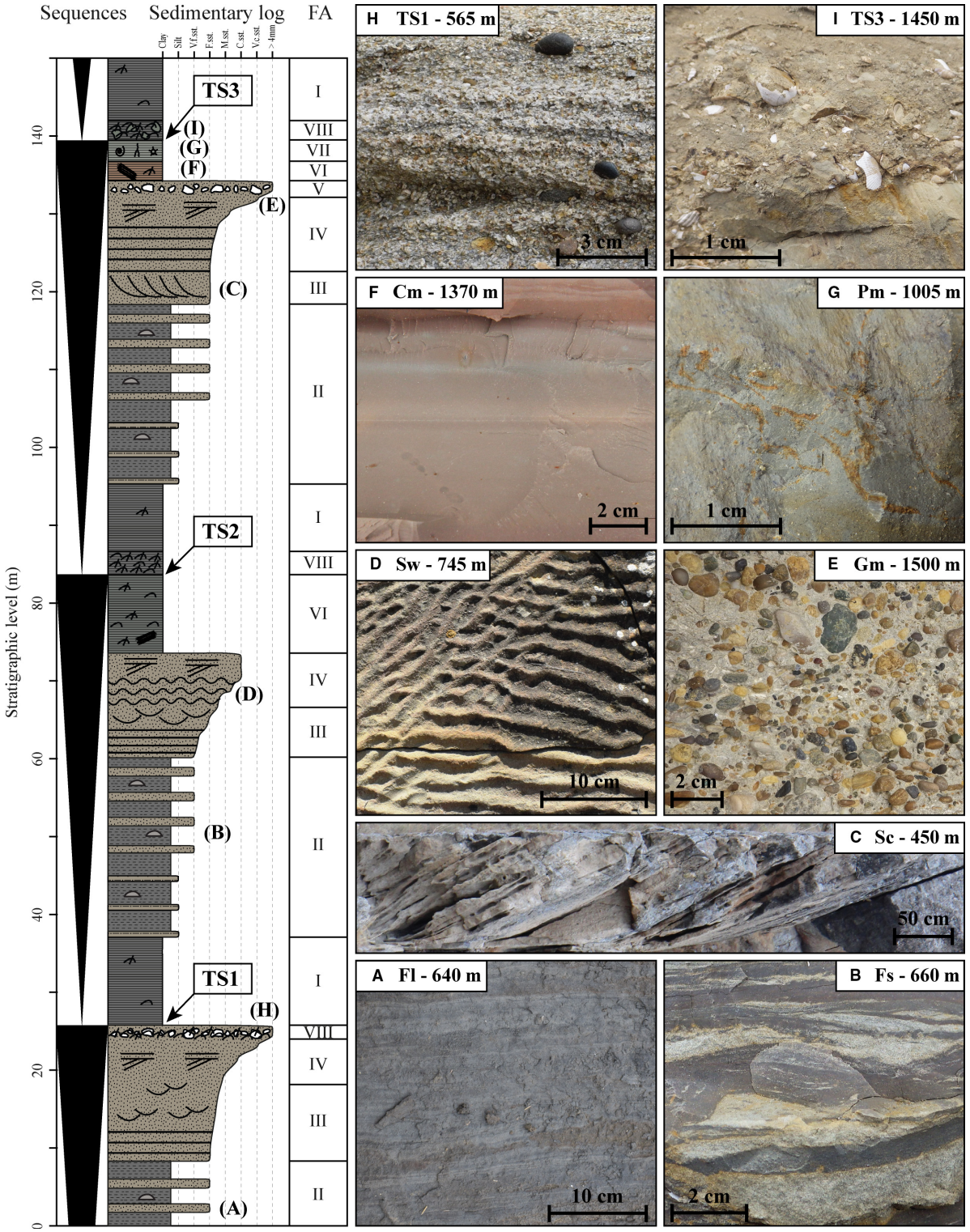

Fig. 4. Model sequences regressing from distal to proximal facies associations. Lithofacies characteristics from each facies association are presented in side view photographs, unless indicated otherwise. (A) Facies Fl: laminated mudstone. (B) Facies Fs: lenticular-bedded mudstone. (C) Facies Sc: Sigmoidal cross-stratified sandstone. (D) Facies Sw: wavy-bedded sandstone (top view). (E) Facies Gm: conglomeratic sandstone. (F) Facies Cm: organic-rich massive mudstone. (G) Facies Pm: Pedogenized massive mudstone. (H) Facies TS1: conglomeratic shell lag. (I) Facies TS2: muddy shell lag.

fluctuations between low energy, open-water conditions and moderate energy bottom-current activities, referenced in the literature as distal storm-generated currents (Héquette & Hill, 1993). Asymmetrical lenticular bedding (Facies Fs) occasionally occurs upward within this facies association, attributed in enclosed environments to intermittent wave action (Reineck & Wunderlich, 1968; de Raaf *et al.*, 1977). Sandstone with trough cross-stratification (Facies St) is known to result from migrations of 2D and 3D sinuous crested dunes (Hamblin, 1961). Sandstone with tabular or sigmoidal cross-stratification (Facies Sc) is interpreted as resulting from migrations of 2D straight crested dunes (Allen, 1963). Sandstone with horizontal planar lamination (facies Sl) is known to be created by upper regime plane-bed flow, under high energy bottom-currents (Cheel, 2006), during redistributing of proximal sediment by storm activity towards more distal depositional settings (Reineck & Singh, 1972). Sediment loading affecting these deposits typically occurs when sandstone is rapidly deposited on top of water-saturated mudstone, leading to fluid expulsion and *in situ* sediment deformations (Oliveira *et al.*, 2009). Reworked shell strings indicate sporadic energy increases, possibly formed as a result of storm activities (Starek *et al.*, 2010; Hampson *et al.*, 2011). Sediment recorded in FA.II highlights variations between low and moderate depositional energies, with energies increasing towards the top as lamina sets and lenses become thicker and more frequent. Deposits are disturbed more repeatedly by moderate wave activity. FA.II represents lower shoreface settings, with sediment deposited between the SWB and the FWB.

Upper shoreface facies association (FA.III)

Description

Facies Association III is composed of 4 to 46 m thick greyish-brown (2·5Y-5/2) fine to coarse-grained sandstone. Sandstone is deposited in 0·5 to 8·0 m thick normal graded beds, with sharp horizontal bases. Sandstone displays four lithofacies types. The first lithofacies consists of sandstone with trough cross-stratification with preserved cross-set thicknesses between 5 cm and 50 cm (Facies St). The second lithofacies is made of sandstone with tabular and sigmoidal cross-stratification with preserved cross-set thicknesses between 5 cm and 50 cm (Facies Sc – Fig. 4C). The third lithofacies is characterized by sandstone with horizontal planar lamination with lamina sets between 1 to 10 mm thick and 1 to 3 mm thick laminae (Facies Sl). The final lithofacies consists of sandstone with swaley cross-stratification, with preserved cross-set thicknesses between 5 cm and 50 cm (Facies Ss). Throughout FA.III, sedimentary structures are commonly draped by fine-grained sediment or millimetre-scale shell fragments. Sandstone beds are occasionally affected by sediment loading. Sediment commonly comprises discontinuous, indurated, 1 to 5 mm thick shell strings with transported shells and shell debris layers. The fauna is composed of a set of lower mesohaline to oligohaline species identified as *Dreissena*, *Apsheronia*, *Monodacna*, *Hyrcania*, *Clessiniola* and *Esperiana* (Appendix S3).

Interpretation

Facies Association III records moderate to high energy depositional energies. Sandstone with trough cross-stratification (Facies St) is known to form by migrations of 2D and 3D sinuous crested dunes (Hamblin, 1961). Sandstone with tabular and sigmoidal cross-stratification (Facies Sc) is interpreted as the result of migrations of 2D straight crested dunes (Allen, 1963). Sandstone with horizontal planar lamination (Facies Sl) is known to result from lower stage plane-bed flow, under high energy bottom-currents (Cheel, 2006), during redistributing of proximal sediment in distal settings during storm activity (Reineck & Singh, 1972). Sandstone with swaley cross-stratification (Facies Ss) is thought to be created under oscillatory waves of high velocity, in shallow waters with low aggradation rates (Dumas & Arnott, 2006). Sediment loading affecting the sandstone indicates its rapid deposition on top of water-saturated mudstone, creating fluid expulsion and *in situ* sediment deformations (Oliveira *et al.*, 2009). Deposition of reworked shell strings indicates relatively high energy depositional environments, attributed in the literature to storm activity (Starek *et al.*, 2010; Hampson *et al.*, 2011). FA.III represents upper shoreface settings, extending from the FWB up to the mean low water level.

Foreshore facies association (FA.IV)

Description

Facies Association IV consists in 1 to 23 m thick intervals dominated by light yellowish-brown (2·5Y-6/3) fine to very coarse-grained sandstone. Sandstone is deposited in 0·5 to 8·0 m thick graded beds, which display sharp horizontal

contacts with underlying sandstone. Sandstone contains three different types of sedimentary structures. The first one consists of horizontal planar lamination made of lamina sets of 1 to 10 mm thick and comprising 1 to 3 mm thick laminae (Facies Sl). Sandstone also contains wavy bedding made of symmetrical ripples with amplitudes of 3 to 5 cm, wavelengths of 7 to 10 cm and preserved cross-set thicknesses between 5 cm and 50 cm (Facies Sw – Fig. 4D). Furthermore, sandstone displays low-angle cross-lamination with preserved cross-set thicknesses between 5 cm and 50 cm (Facies Sa). Throughout FA.IV, laminae are commonly draped by finer-grained sediment or millimetre-scale shell fragments. Sandstone contains abundant continuous 1 to 10 cm thick erosive layers of transported shell debris and shells. Layers display mixed assemblages of mostly oligohaline genera, with *Dreissena*, *Apsheronia*, *Monodacna*, *Hyrcania*, *Didacna*, *Corbicula*, *Clessiniola*, *Theodoxus* and *Laevicaspia* (Appendix S3).

Interpretation

Facies Association IV represents high energy depositional energies. Sandstone with horizontal planar lamination (Facies Sl) is documented to be created by lower stage plane-bed flow regime, under high energy bottom-currents (Cheel, 2006) and found in the attenuated wave zone along the coastline (Martel & Gibling, 1991). Sandstone with wavy bedding (Facies Sw) is recognized as being formed under stationary wave oscillations, affecting the sediment floor (de Raaf *et al.*, 1977). Sandstone with low-angle cross-lamination (Facies Sa) is linked to migration of low relief dunes, under swash and backwash currents, during half-stationary wave oscillations impacting the sediment floor (de Raaf *et al.*, 1977). FA.IV represents foreshore settings, extending from the mean low up to the mean high water level, subjected to daily wave swash.

Backshore facies association (FA.V)

Description

Facies Association V is composed of 1 to 7 m thick intervals dominated by light yellowish-brown (2·5Y-6/3) medium to very coarse-grained sandstone. Sandstone is deposited in 0·2 to 1·0 m thick graded beds, with sharp horizontal lower contacts. Sandstone contains two lithofacies types. The first lithofacies is dominated by sandstone with horizontal planar lamination made of lamina sets 1 to 10 mm thick and comprising 1 to 3 mm thick laminae (Facies Sl). The second lithofacies consists of conglomeratic sandstone (Facies Gm – Fig. 4E). Sandstone is matrix-supported and contains common millimetre-scale lithic pebbles, glauconite grains and mud clasts, as well as abundant reworked oligohaline molluscs and rare reworked Neogene planktonic foraminifera (Fig. 5A and B). These two lithofacies display sandstone with low compositional maturity, because it is mostly composed of quartz and feldspar grains, and highlights high textural maturity, as it comprises well-sorted and rounded grains presenting moderate-sphericity. These deposits occasionally contain shell pavements, displaying partial or total cementation of the grains in a post-diagenetic carbonate matrix (Fig. 5C and D). Shell pavements contain mixed assemblages with oligohaline species of *Dreissena*, *Apsheronia*, *Monodacna*, *Hyrcania*, *Didacna*, *Corbicula*, *Clessiniola*, *Theodoxus*, *Laevicaspia* and *Turricaspia* (Appendix S3).

Interpretation

Facies Association V represents very high depositional energies. Sandstone with horizontal planar lamination (Facies Sl) is considered to represent lower stage plane-bed flow regime, under high energy bottom-currents (Cheel, 2006) and is found in the attenuated wave zone along coastlines (Martel & Gibling, 1991). Shelly conglomeratic sandstone (Facies Gm) is recognized as a lag deposit, formed under very high energy wave reworking in the swash zone (Bourgeois & Leithold, 1984). It may form shell pavements when undergoing post diagenetic dissolution, identified as the main mechanism of formation for beach cement (Kneale & Viles, 2000). Such beach rocks typically represent very high energy sediment reworking and winnowing (Kidwell & Aigner, 1985). The lateral continuity of indurated sandstone layers, parallel to the palaeocoastline, points towards the absence of mouth bars or tidal inlets, and the presence of a continuous low-relief coastline. FA.V represents backshore settings, extending from the mean high water level up to the highest storm level, where reworking and winnowing are affecting sediment deposition.

Lagoonal facies association (FA.VI)

Description

Facies Association VI is composed of 1 to 22 m thick alternations between olive brown (5Y-4/3)

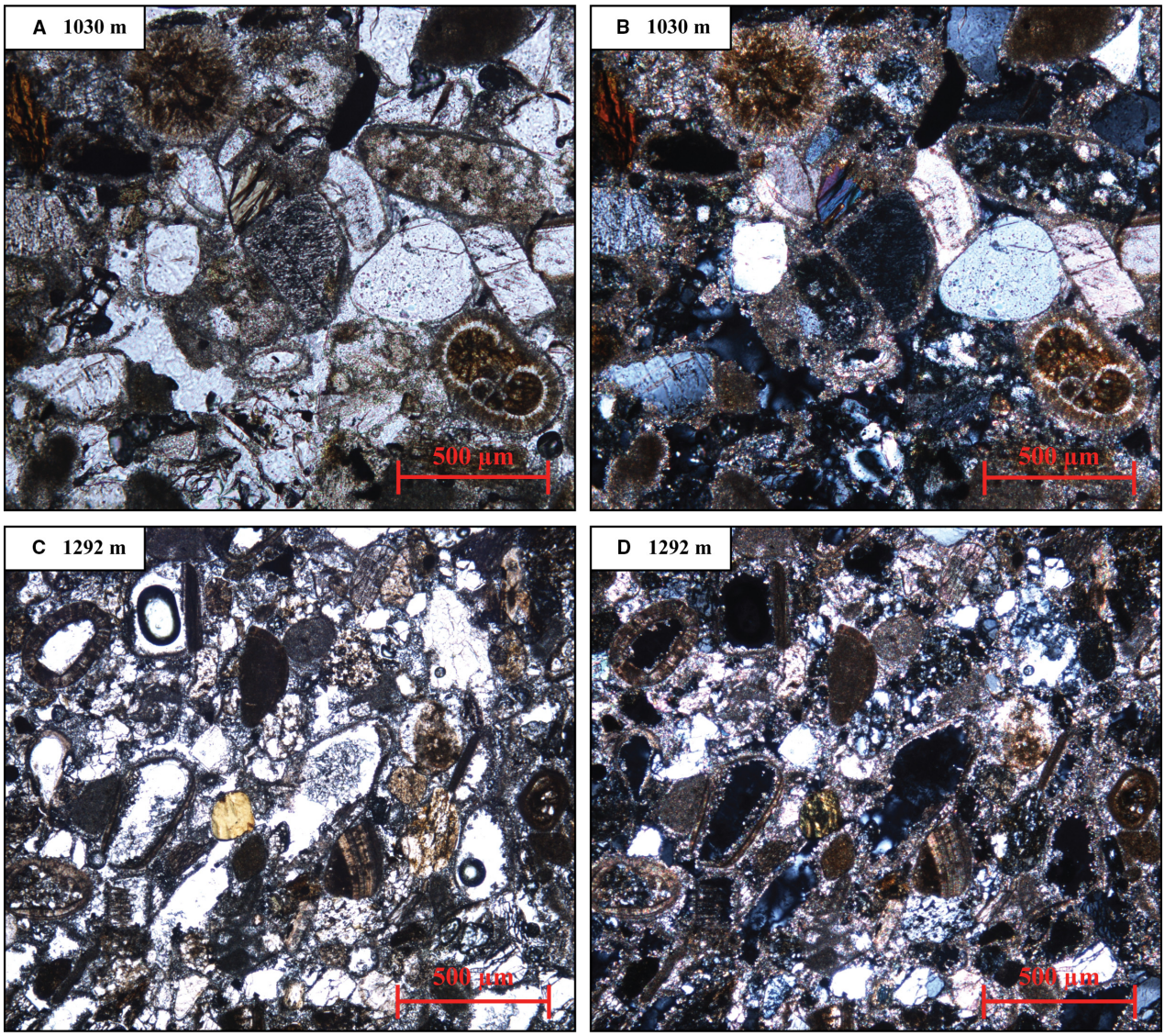

Fig. 5. Thin-section photographs of coastal sediments deposited in the Palaeo-Kura Basin including glauconite grains, abraded shell fragments and reworked foraminifera. Non-indurated beach deposits: (A) under polarized light; and (B) under polarized and analysed light. Indurated beach deposits enclosed within a post-diagenetic calcite matrix (C) under polarized light (D) under polarized and analysed light.

sandstone and olive-grey (5Y-4/2) or reddish-brown (5YR-4/3) mudstone. Massive mudstone (Facies Cm – Fig. 4F) is present in 1 to 5 m thick intervals. It randomly alternates with 1 to 15 m thick mudstone with horizontal planar silt lamination, made of lamina sets 0·5 to 3·0 cm thick and comprising 1 to 3 mm thick laminae (Facies Cl). Sediment also contains 0·5 to 5·0 m thick light yellowish-brown (2·5Y-6/3), very fine to medium-grained sandstone beds. Sandstone presents horizontal planar silt lamination with lamina sets 1 to 10 mm thick and 1 to 3 mm thick laminae (Facies Cs). Massive and laminated mudstones are occasionally affected by centimetre-scale depositional faults. Throughout FA.VI, sediment contains abundant millimetre to centimetre-scale terrestrial organic material fragments. It also displays common vertical roots 1 to 5 cm long and 0·1 to 0·3 cm wide and rare vertical burrows 1 to 3 cm long and 0·3 to 0·5 cm wide. Sediment is occasionally affected by reddish oxidation. Furthermore, it contains sporadic 1 to 5 cm thick white chalk layers, enriched in charophytes and fish bones. Mudstone commonly contains dispersed *in situ* freshwater to oligohaline molluscs, including

Dreissena, *Apsheronia*, *Monodacna*, *Corbicula*, *Laevicaspia*, *Esperiana*, *Lymnaea*, *Valvata*, *Theodoxus*, *Planorbis*, *Unio* and *Bythinia* (Appendix S3). The same genera are only rarely present in sandstone, where they are reworked in centimetre-thick layers.

Interpretation

Facies Association VI records alternations between very low and moderate depositional energies in organic-rich environments. Organic-rich massive mudstone (Facies Cm) is recognized to be deposited from suspension in very low energy standing waters (Link & Osborne, 1978; van de Velde *et al.*, 2019). Mudstone with horizontal planar silt lamination (Facies Cl) is typically documented as overbank deposition during washover events (Schwartz, 1982). Sandstone with horizontal planar silt lamination (Facies Cs) is known to be deposited during intermittent increases of energy disrupting very low energy standing waters and is linked to occasional overbank deposition during washover storm events of higher energy (Schwartz, 1982). FA.VI records organic-rich and well-oxygenated environments, interpreted as lagoonal settings.

Terrestrial floodplain facies association (FA.VII)

Description

Facies Association VII consists of 1 to 10 m thick reddish-brown (5YR-4/3) or greenish-grey (GLEY1-6/10GY) mudstone. The succession contains 1 to 5 m thick massive pedogenized mudstone intervals (Facies Pm – Fig. 4G). They are irregularly intercalated by 1 to 10 m thick pedogenized mudstone with horizontal planar lamination of silts to very fine sands (Facies Pl). Lamina sets are 0·5 to 1·0 cm thick and comprise 1 to 3 mm thick laminae. Mudstone contains rare *in situ* freshwater molluscs, such as *Corbicula*, *Melanoides*, *Unio* and *Planorbis* (Appendix S3). Mudstone contains various scales of slickenslides, reddish and greenish colour mottling, and development of blocky peds. It commonly contains millimetre-scale organic material fragments, vertical roots 1 to 5 mm long and 0·1 to 0·3 cm wide, as well as vertical burrows 1 to 3 cm long and 0·3 to 0·5 cm wide.

Interpretation

Facies Association VII represents alternations between very low and low depositional energies. Pedogenized mudstone (Facies Pm) is suggested to be deposited from suspension in very low energy standing waters (Link & Osborne, 1978). Pedogenized laminated mudstone with horizontal planar lamination (Facies Pl) is typically documented as overbank deposition during washover events (Schwartz, 1982). The presence of mottling and slickenslides represents pedogenesis (Retallack, 2001; Kraus & Hasiotis, 2006). FA.VII displays organic-rich environments, subject to subaerial exposure and pedogenesis, and is interpreted as terrestrial floodplain settings.

Transgressive facies association (FA.VIII)

Description

Facies Association VIII consists of a 0·1 to 0·5 m thick shelly interval, expressed in three different manners according to its stratigraphic relation with neighbouring facies associations. Facies Association VIIIa occurs on top of backshore deposits (FA.V – see *Backshore facies association* section). It consists of erosive shelly intervals made of light yellowish-brown (2·5Y-6/3), medium to very coarse-grained sandstone (Facies TS1 – Fig. 4H). Shelly sandy deposits form condensed layers that contain abundant millimetre-scale, well-sorted, abraded shell fragments. Faunal assemblages record mixed salinities from freshwater to oligohaline. These layers include millimetre-scale glauconite grains and centimetre-scale lithic pebbles, moderately sorted, well-rounded and with moderate-sphericity.

Facies Association VIIIb is deposited in the upward continuity of lagoon deposits (FA.VI – see *Lagoonal facies association* section). It displays a gradual faunal change in a muddy matrix (Facies TS2). The matrix records a transition from olive-grey (5Y-4/2) or reddish-brown (5YR-4/3) to dark bluish-grey (GLEY2-4/5B) or dark greenish-grey (GLEY1-4/5G) mudstone. The base of FA.VIIIb displays abundant, moderately-sorted shells and shell fragments, representing freshwater to mesohaline salinities. Towards the top, deposits only present some dispersed, well-sorted shells, characteristic for mesohaline to oligohaline salinities.

Facies Association VIIIc is deposited on top of terrestrial deposits (FA.VII – see *Terrestrial floodplain facies association* section). It documents erosive shelly intervals made of dark bluish-grey (GLEY2-4/5B) to dark greenish-grey (GLEY1-4/5G) mudstone (Facies TS3 – Fig. 4I). The muddy matrix contains reddish-brown (5YR-4/3) to greenish-grey (GLEY1-6/10GY)

mudstone pebbles. Mudstone pebbles are centimetre-scale, very poorly-sorted, very angular and with low-sphericity. Clast composition is similar to the eroded underlying sediment. Deposits are enriched in abundant abraded shells and shell fragments.

Interpretation

Facies Association VIII represents transitional intervals from backshore, lagoonal or terrestrial settings to offshore settings (FA.I – see *Offshore facies association* section). Facies Association VIIIa highlights an energetic and rapid deepening on top of backshore deposits, generating sediment erosion, reworking and winnowing. Similar sandy shelly lag deposits have previously been interpreted as erosional ravinement surfaces (Kidwell & Aigner, 1985; Scarponi *et al.*, 2013). Facies Association VIIIb displays a less energetic and more gradual deepening on top of lagoonal deposits, leading to increasing salinity associated with a reduction in the amount of shells. Even if no ravinement surface has been observed in the field, these gradual changes in faunal assemblages are interpreted as transgressive events, also referred to as progressive and transgressive overlap (Grabau, 1906). Facies Association VIIIc represents an energetic and rapid deepening on top of terrestrial deposits, producing sediment erosion and reworking. Similar muddy shelly lag deposits have previously been interpreted as erosional transgressive surfaces (Driese & Foreman, 1991). In brief, FA.VIII represents sudden transgressive events of offshore settings on top of backshore, lagoonal or terrestrial settings.

Stratigraphic architecture

Within the Apsheronian interval, facies associations are repeatedly deposited following the same stratigraphic order, forming sedimentary successions recurrently regressing from distal to proximal depositional environments. Sedimentary successions start with *ca* 9 m of bluish-grey to greenish-grey mudstone deposited in offshore settings (FA.I). Upward, they record *ca* 15 m of alternating greenish-grey mudstone and greyish-brown very fine to medium-grained sandstone representing lower shoreface settings (FA.II). Fine to coarse-grained greyish-brown sandstone with small-scale sedimentary structures becomes increasingly dominant over mudstone illustrating *ca* 14 m of upper shoreface settings (FA.III). Sedimentary successions continue with *ca* 7 m of fine to very coarse-grained greyish-brown sandstone with larger-scale sedimentary structures representing foreshore settings (FA.IV). Upward, *ca* 2 m of medium to very coarse-grained yellowish-brown sandstone with low-angle sedimentary structures is found illustrating backshore settings (FA.V). Palaeocurrent directions measured on cross-sets in foreshore and backshore depositional settings and corrected for the bedding planes highlight mean unidirectional dip directions between 180° and 210°, with 65% of all palaeocurrent dip directions recorded within a range from 150° to 240° (Fig. 6). Sedimentary successions are sometimes overlain by *ca* 6 m of brownish lagoonal mudstone (FA.VI), occasionally overlain by *ca* 5 m of reddish or greenish terrestrial mudstone (FA.VII). Each sedimentary succession corresponds to a regressive sequence, prograding southward from offshore up to coastal, lagoonal or continental environments. Regressive sequences are overlain by conglomeratic shell lags on top of backshore deposits (FA.VIIIa), transitional shelly mudstone on top of lagoon deposits (FA.VIIIb) or muddy shell lags on top of terrestrial deposits (FA.VIIIc) that represent flooding events. Repeated transgressive events on top of regressive sequences highlight recurrent relative lake-level variations whose amplitudes are discussed below.

Relative lake-level variations display repetitive patterns throughout the section. In total, 20 regressive cycles, separated by 20 highstands, were found approximately every 60 ± 50 m along the facies depth rank (Fig. 3C). As the amplitude of regressive sequences is rather constant, this suggests no major environmental change throughout the entire sedimentary record, such as the substantial deepening recorded in the Plio-Pleistocene Akchagylian regional stage (van Baak *et al.*, 2019). The very good preservation of sequences, aggrading under unidirectional and non-erosive depositional processes, attests to their deposition during normal regressions and in sufficient accommodation space. Regression events are overlain by major erosive flooding surfaces, formed under rapid lake-level increases of high amplitude. The amplitude of these sudden transgressive events probably prevented the formation of transgressive system tracts on top of the flooding surfaces. The regularity of these repeated lake-level fluctuations, shaping 20 sequences formed under normal regression and sediment aggradation, demonstrate the lack of significant subsidence

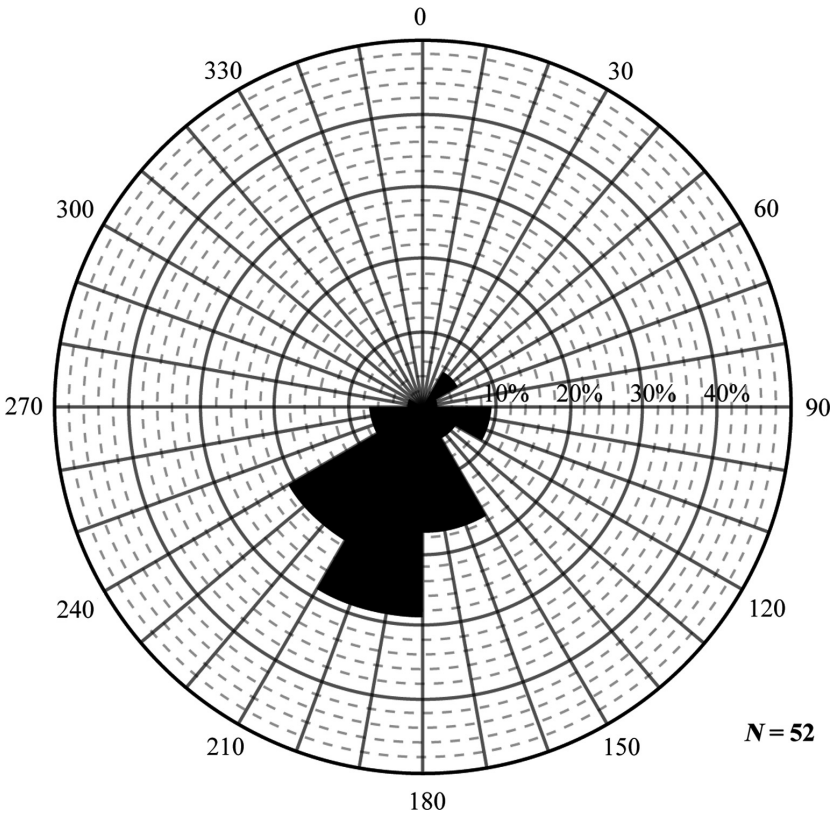

Fig. 6. Palaeocurrent measurements on three-dimensional cross-beds of backshore sedimentary structures along the Hajigabul section display palaeocurrent directions flowing southward perpendicular to the coast of the Palaeo-Kura Basin (n = 52).

rise, loss of sediment supply or lake-level drop (Posamentier *et al.*, 1998). Instead, it points towards high sediment supply continuously balanced by high subsidence rates, overruled by repeated transgressive events along the coastline, whose recurrence is driven by external forcing mechanisms.

Timing of environmental changes

Frequency of relative lake-level variations may be assessed along the Hajigabul section thanks to its rather well-constrained age model. By correlating the six existing magnetostratigraphic age tie points with the geomagnetic polarity timescale (Gradstein *et al.*, 2012), the exposed sedimentary record, deposited between 550 m and 1630 m, is dated from *ca* 2·1 to 0·85 Ma (Lazarev *et al.*, 2019). Based on this time frame, sedimentation rates were extrapolated and the interval of interest, recording repeated lake-level fluctuations between 400 m and 1615 m, is dated from *ca* 2·3 to 1·2 Ma (Fig. 7A). Considering this entire interval, the 20 lake-level highstands display an average frequency of *ca* 53·3 kyr. However, the age model is not as equally robust along this interval. The lower part of the section (150 to 510 m) and the upper part of the section (1100 to 1700 m) only document two age tie points each. With the presence of four age tie points, the stratigraphically continuous middle part of the section (510 to 1100 m) displays a very robust time frame and records a sedimentation rate of *ca* 1·54 m kyr^{-1}. Based on this very well-constrained interval, the nine lake-level highstands occur with an average frequency of *ca* 41·1 kyr, in the range of the 41 kyr obliquity cycles.

A Blackman-Tukey transformation of the lake-level curve realized along this interval to the time domain reveals spectral power at frequency 0·0195069 and bandwidth 0·00827091 with 90% confidence. Spectral analyses result in a large number of peaks with a dominant one between 36 kyr and 89 kyr. The applied 36 to 89 kyr bandpass filter depicts the lake-level cycle well, apart from two cases (Fig. 7B). In the first case, the filter shows peaks that are not present in the

lake-level curve. One extra cycle occurs in the filter between highstand 1/2, and one after highstand 20. This may be due to the poorly constrained age model in the lowermost and uppermost parts of the section. In the second case, the filter groups cycles 7/8, and cycles 11/12 into one. The frequency of these highstands is too high to be picked up by the filter. The age model is not able to resolve whether these highstands relate to different forcing or whether these were potentially deposited under lower sedimentation rates. Except for these two cases, the representability of lake-level variations by the bandpass filters is very high.

When plotted against one another, lake-level highstands match relatively well to obliquity maxima within the freedom of the age model (Fig. 7C). The additional cycles created by the filters in time and cycle domains between highstands 1/2, and above highstand 20, are similarly present in the obliquity curve. The two cycles banded together by the filters between highstands 7/8 and 11/12 are ungrouped due to the lower sedimentation rates. Two additional cycles are created between highstands 13/14 and 18/19 due to the higher sedimentation rates. Even if some dissimilarities are documented, the correlation between lake-level variations, bandpass filters and obliquity cycles is rather high. The relative lake-level curve also appears in the range of global sea-level changes (Fig. 7D). Consequently, Early Pleistocene lake-level in the Kura Basin appears to have been sensitive to 41 kyr obliquity cycles, driving ice-volume and global sea-level.

DISCUSSION

Sedimentary architecture of the Kura Basin palaeocoastline

The architecture of sediment deposited along the northern margin of the Kura Basin during the Early Pleistocene Apsheronian regional stage records repeated Caspian Sea incursions within this embayment (Fig. 1A). The facies model of the coastal sedimentary successions deposited in this bay displays several features typically generated under wave activity. Sediment regularly documents planar-lamination formed by storm-generated currents, transporting proximal sediment towards more distal depositional settings (Héquette & Hill, 1993). Deposits commonly display wavy bedding, low-angle cross-lamination and swaley cross-stratification, generated under oscillatory wave action (de Raaf *et al.*, 1977; Dumas & Arnott, 2006; Ainsworth *et al.*, 2011). Sediment frequently contains shelly beach rock, formed by wave reworking and winnowing in the swash zone (Bourgeois & Leithold, 1984; Davis & Hayes, 1984; Kidwell & Aigner, 1985). Upward, washover deposits occur, formed under wave reworking (Davis & Hayes, 1984).

Some characteristic features of wave-dominated coastlines nevertheless have not been found. Wave-dominated systems commonly contain sedimentary structures generated under longshore currents (Davis & Hayes, 1984). Longshore sediment drifting typically leads to the formation of barrier bars and spits (Bhattacharya & Giosan, 2003), commonly observed along the restricted Mediterranean, Black Sea and Caspian Sea (van der Meulen & Salman, 1996; Lahijani *et al.*, 2009, 2019; Matishov *et al.*, 2013; Vespremeanu-Stroe *et al.*, 2017). These structures usually include varied current directions (Nielsen & Johannessen, 2009). Apsheronian sediment is still deposited under quite unidirectional palaeocurrent directions, flowing to the south-west (Fig. 6), perpendicular to the Kura Basin palaeocoastline oriented north-west/south-east (Fig. 1B). Moreover, sediment does not record any aeolian influx, typically found along barrier bars and spits (Davidson-Arnott & van Heyningen, 2003). Such structures document limited lateral continuity (Davidson-Arnott & van Heyningen, 2003). In the Kura Basin, however, sediment bodies may be traced over at least 4 km laterally on aerial photographs of the Hajigabul anticline (Fig. 8). Although most features

Fig. 7. The depositional record of lake-level change in the Hajigabul section during the Early Pleistocene. (A) Reconstructed lake-level curve in time domain estimated by the facies depth rank. (B) Bandpass filters generated along the lake-level curve in time domain. (C) Milankovitch astronomical target curve of obliquity (Laskar *et al.*, 2011). (D) Global sea-level curve (de Boer *et al.*, 2014). In order to discuss the simultaneous evolution of these four curves, the time frame of the section (Lazarev *et al.*, 2019) is plotted by dotted black lines against the geomagnetic polarity timescale (Gradstein *et al.*, 2012). The yellow lines highlight the intervals between magnetostratigraphic sample levels and the orange striped interval displays the hiatus present at the top of the section.

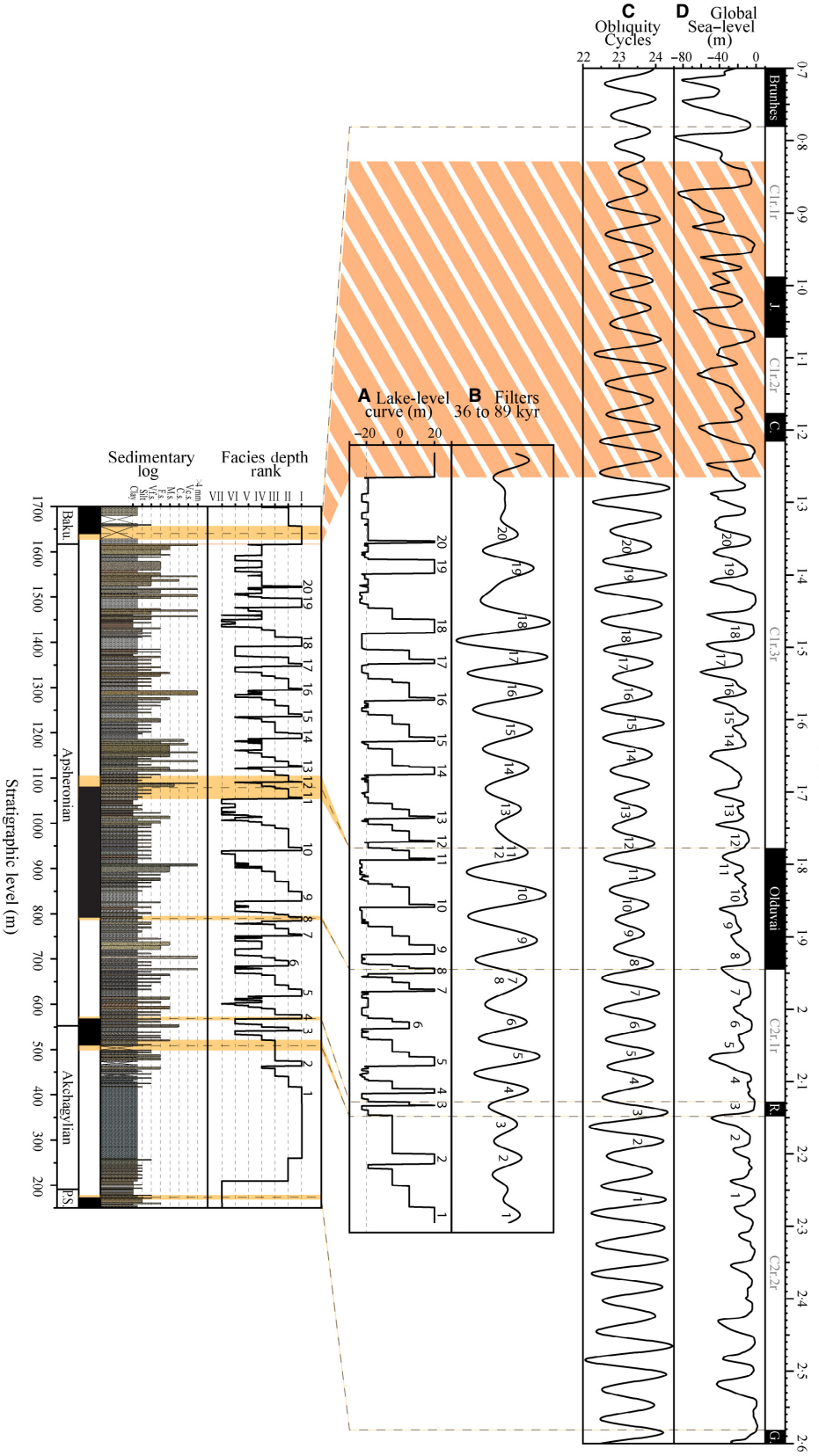

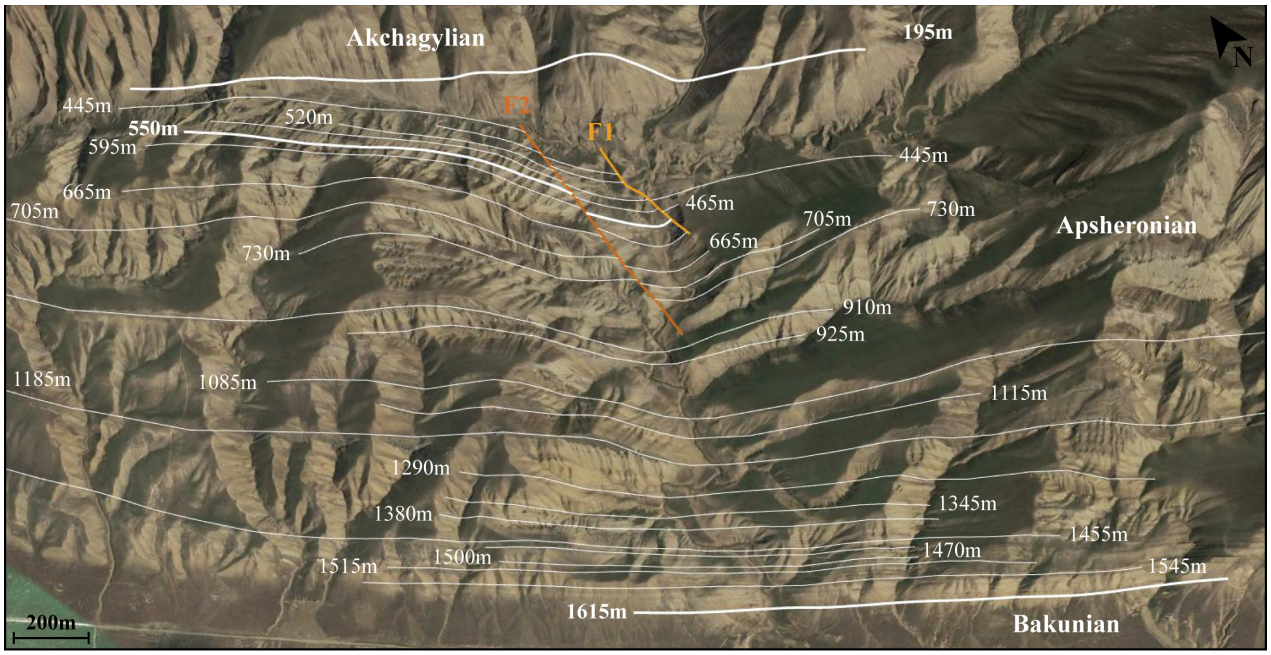

Fig. 8. Aerial photograph of the Hajigabul section from Google Earth® with mapping of the regional stages boundaries, the two strike-slip faults F1 and F2 and some of the most characteristic layers, emphasizing their lateral continuity over distances of at least 4 km along the anticline.

point to a wave-dominated coastal architecture, some dissimilarities exist compared to typical wave-dominated coastlines.

Fluvial influence along the northern coastline of the Kura Basin appears to have been rather limited. Sandstone layers do not display major fluvial features such as strong basal erosive or channelization typical of fluvial channels. Sandstone bodies are laterally continuous and are conformably deposited on top of underlying sediment. Additionally, sediment lacks fluvial evidence such as high-angle trough cross-stratification (Ainsworth *et al.*, 2011), hyperpycnal flows or enrichment in terrestrial organic material (Jorissen *et al.*, 2018). Sediment input originates from small northern sources with limited impact on the coastal morphology. Deposits yield evidence for a northern sediment source with palaeocurrents flowing southward, offshore from the northern margin of the Kura Basin.

Due to the isolation of the Kura Basin from the open ocean, its coastline did not experience any tide activity. Sediment does not contain characteristic tidal deposits, such as swash sedimentary structures, intertidal clay-drape couplets (de Boer *et al.*, 1988), intensive bioturbation in foreshore sediment, or extensive development of current ripples below the fair-weather wave base (FWB) (Frey & Dashtgard, 2011). These features are typically recorded within foreshore sediment, deposited between the mean low tide and mean high tide in open marine environments. However, isolated basins usually display extremely low tidal ranges, and foreshore deposits represent in this case a transitional interval between mud-dominated shoreface and sand-dominated backshore settings, lacking indications for tide activity.

Wind action along the coastline also appears to have been limited, with a lack of major storm winds. The documented succession lacks any evidence of strong wind-induced features such as aeolian beach deposits (Otvos, 2000) or sediment resuspension (Booth *et al.*, 2000). The northern coastline of the Kura Basin appears to have been protected by the Greater Caucasus from the strong northern winds recorded nowadays around the Caspian Sea (Kosarev, 2005). In brief, the northern margin of the Early Pleistocene Kura Basin shaped a straight wave-dominated coastline, rather dissimilar to those in the open ocean due to the lack of tide activity, or any major fluvial or aeolian interference.

Along this protected coastline, wave energy was less significant than in typical wave-dominated systems. With average wave heights of

0·25 m during calm seas and 1 to 4 m during storm events (Terziev *et al.*, 1992; Amirinia *et al.*, 2017), this coastline is in fact classified as a low energy wave-dominated beach (Jackson *et al.*, 2002b). Following recognized beach classifications (Short, 2006), the sedimentary architecture of the Kura Basin palaeocoastline is ranked as a low energy wave-dominated reflective beach. The low reflectivity of such coastlines enhances offshore sediment transport and increases sediment accretion. With a sedimentation rate around 1·5 m kyr^{-1}, the Kura Basin coastline recorded rapid aggradation. Reflective beaches are generally composed of relatively coarse sandstone due to waves breaking closer to the shoreline (Short, 2006). Similarly, the studied sedimentary succession is composed of relatively coarse grains. Moreover, such coastlines are characterized by very narrow or even completely absent surf zones (Aagaard *et al.*, 2013). The Apsheronian coastline probably formed such a narrow and steep beach, since it was situated along the northern margin of the foreland basin of the Greater Caucasus. However, if proximal backshore settings were relatively narrow and steep, distal foreshore, shoreface and offshore settings were rather wide and shallow. The steepness of the distal palaeocoastline was undoubtedly scaled down compared to the present-day southern Iranian coast of the Caspian Sea (Kosarev, 2005) or compared to beaches along the open ocean (Short, 2006). The succession misses the deposition of major mass-transport deposits, typical for deep and steep shelves (Postma, 1995), steeply dipping sedimentary structures or erosional chutes (Orton & Reading, 1993). The Kura Basin shaped in fact a shallow, protected and restricted embayment of the Caspian Sea. The basin was filled in by sediment originating from the northern Greater Caucasus and from the Kura Delta confined further to the west (Mamedov, 1997; Hoogendoorn *et al.*, 2005; Abreu & Nummedal, 2007). Sediment was probably transported, washed and deposited under weak river and wave action along the northern margin of the Kura Basin. While this study provides a good analogue for a protected wave-dominated coast, additional research is still needed to fully assess sedimentary architecture within a basin devoid of major tide and wave activity.

Amplitude of Early Pleistocene Caspian Sea lake-level variations

In enclosed basins, with limited tide and wave activity, facies association boundaries are delimited between wave baselines and/or water levels that are expected to be shallower than in the open ocean. Waves in the present-day offshore Caspian Sea typically display wavelengths around 50 m during storm events (Hartgerink, 2005). The storm-wave base (SWB) (offshore – lower shoreface transition), situated at a depth of half the wavelength, would consequently be located at maximum 25 m water depth. Following the same approach, with average wavelengths estimated around 32 m (Hartgerink, 2005), the FWB (lower – upper shoreface transition) would be situated at maximum 16 m water depth. Within oceanic settings the lowest SWB lies between 20 m and 200 m water depth, and the FWB between 5 m and 20 m water depth (Nichols, 2009). Furthermore, in the Caspian Sea, the mean low and high water levels are mostly driven by seasonal variations in evaporation, precipitation and runoff, acting on the water budget of this endoreic basin (Degens & Paluska, 1979; Kroonenberg *et al.*, 1997). Such seasonal fluctuations generate lake-level variations up to ±0·2 m amplitude in the present-day Caspian Sea (Chen *et al.*, 2017). The mean low water level (upper shoreface – foreshore transition) would consequently be situated around −0·2 m and the mean high water level (foreshore – backshore transition) around +0·2 m. Such levels are very dissimilar compared to oceanic systems, where tidal ranges display variations between ±1 m and ±7 m amplitude (Nichols, 2009). Finally, waves are between 1 to 4 m high during storm events in the present-day Caspian Sea (Terziev *et al.*, 1992; Amirinia *et al.*, 2017). The highest storm level (backshore – continental transition) would therefore be situated at maximum +4 m. In oceanic settings, waves may reach up to 12 m height during storm events (Bouws *et al.*, 1996).

Consequently, offshore sediment in the Kura Basin would be found between approximately −40 m and −25 m, lower shoreface sediment between −25 m and −15 m, upper shoreface sediment between −15 m and −0·2 m, foreshore sediment between −0·2 m and +0·2 m, and backshore sediment above +0·2 m. Lagoonal and continental sediment would be deposited around 0 m, behind the beach barriers (Fig. 9). However, elongated bays like the Kura Basin usually attenuate the energy of wave influx (Caliskan & Valle-Levinson, 2008). The facies boundaries may have been shallower in the Kura Basin, shielded from major storm, wave and wind activity by the eastern Caucasus extension. Nevertheless, without any additional

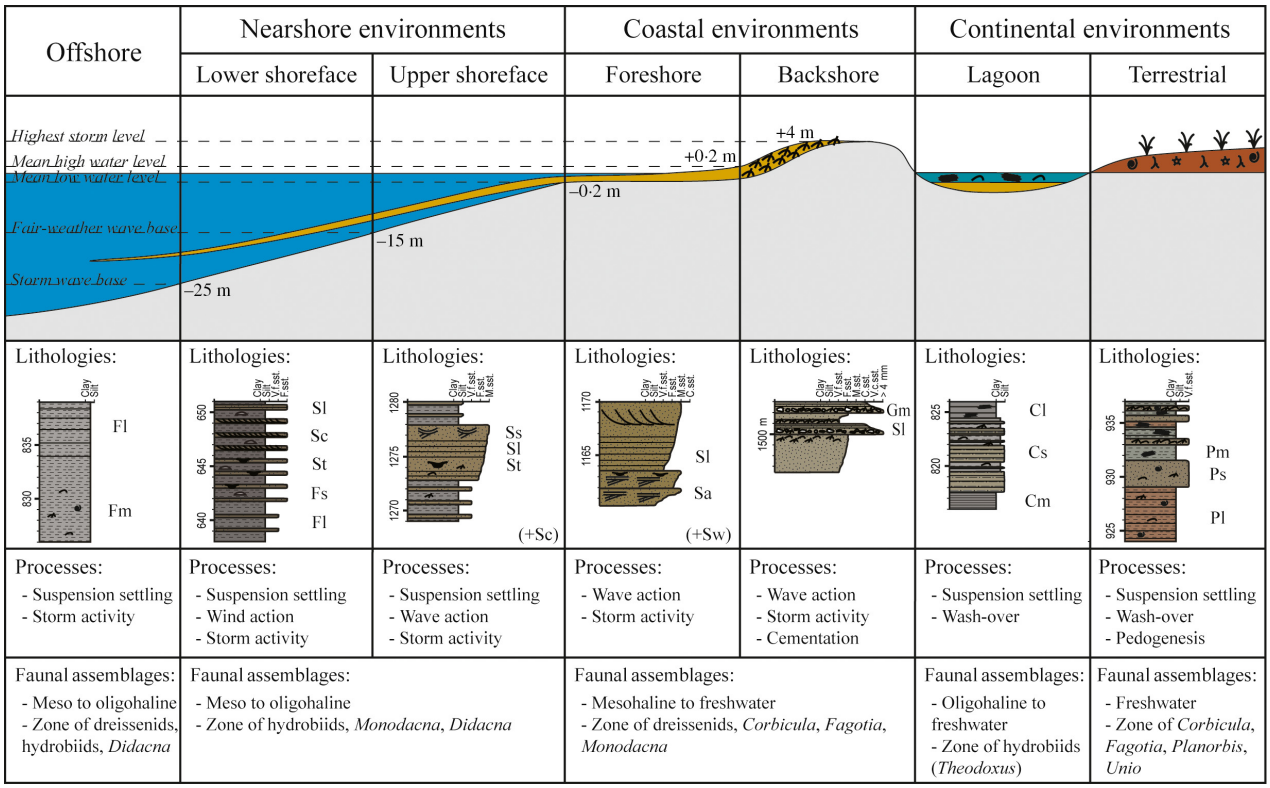

Fig. 9. Summary of facies associations, depositional processes and faunal assemblages, illustration of lateral relationships in between the different depositional environments and the relative water depth of facies association boundaries.

information like characteristic ichnofossils or robust subsidence rate studies, it remains extremely challenging to provide absolute water depths for these facies boundaries. For now, relative lake-level variations are approximated to oscillate between −40 m and 0 m relative water depth.

Water levels in the Early Pleistocene Kura Basin may be estimated based on the assumption that surface levels were not tectonically elevated or depressed compared to the present-day topography. During lowstands, the western and middle part of the Kura Basin recorded terrestrial environments (Agustí *et al.*, 2009; Krijgsman *et al.*, 2019), the eastern part documented offshore environments (van Baak *et al.*, 2013) and the northern margin of the basin recorded coastal, lagoonal and terrestrial environments (Fig. 10A). At −20 m, the water level would have been 8 m above today's absolute water level. This 8 m water increase compared to the present-day would have been enough to flood the easternmost part of the Kura Basin, keep the westernmost part emerged and only have limited impact on its northern margin, where littoral environments could have developed. During highstands, the western part of the Kura Basin still recorded terrestrial environments (Krijgsman *et al.*, 2019) and the eastern part still documented offshore environments (van Baak *et al.*, 2013). However, repeated alternations between terrestrial and nearshore environments were recorded in the middle part of the basin (Nevesskaja, 2007; Krijgsman *et al.*, 2019) and along its northern margin (Fig. 10A). At +20 m, the water level would have been 48 m above today's absolute water level. Following such a water level increase compared to present-day, highstands would not have reached the far western end of the basin still recording terrestrial settings, while the middle part of the basin and its northern margin would have been episodically flooded, and the eastern part of the basin would have been constantly flooded. Early Pleistocene lake-level variations in the Kura Basin consequently oscillated with an amplitude of *ca* 40 m, between water levels −20 m and +20 m (Fig. 10B).

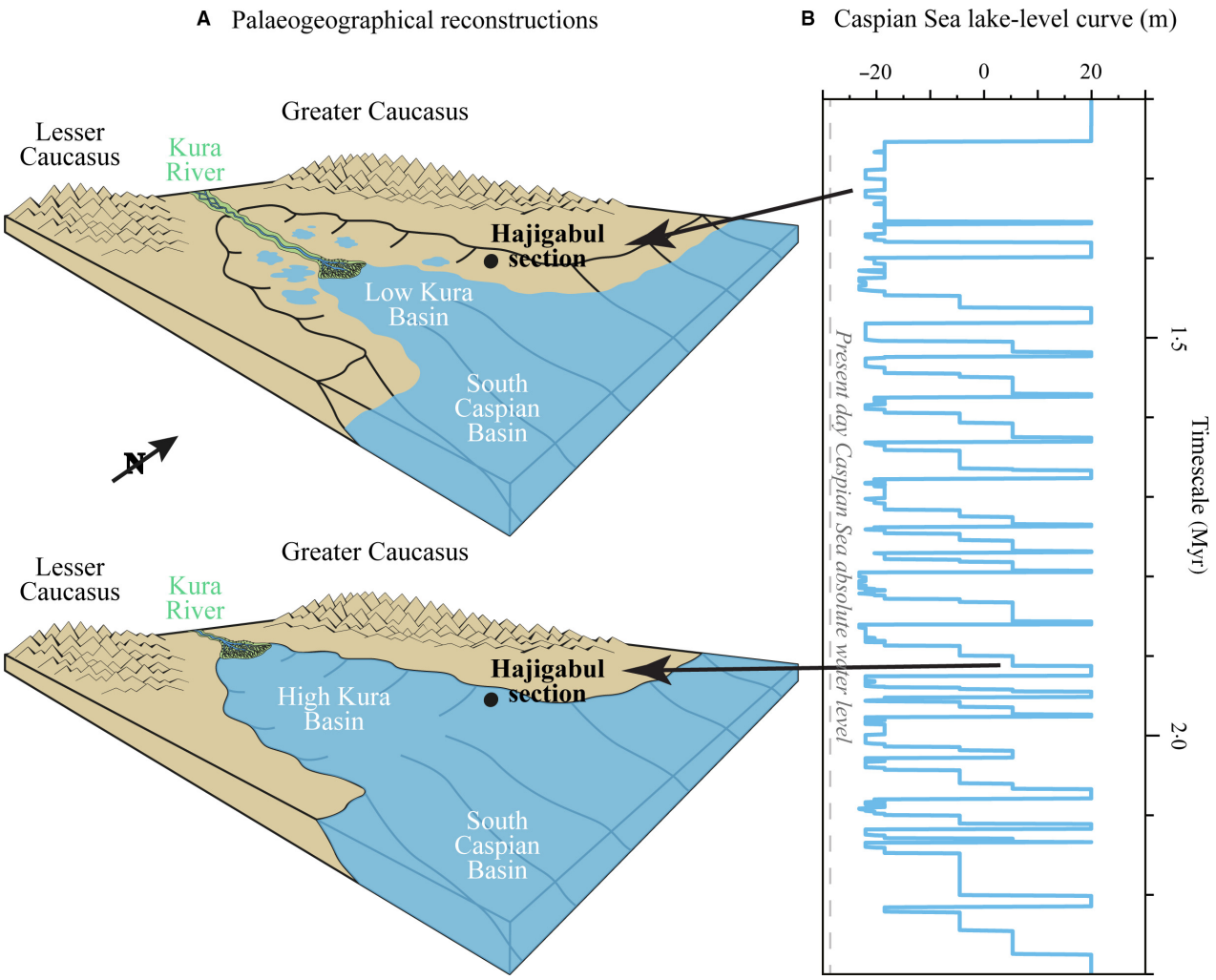

Fig. 10. Environmental reconstruction of the Caspian Sea during the Early Pleistocene Apsheronian regional stage. (A) Palaeogeographical reconstructions of the Kura Basin during Caspian Sea lowstands and highstands. (B) Caspian Sea lake-level curve repeatedly oscillating between −20 m and +20 m.

Drivers of Early Pleistocene Caspian Sea lake-level changes

Lake-level fluctuations, as recorded laterally over at least 4 km in the Kura Basin, are similarly observed along nearby sections further to the north-east along the Caspian Sea coast (Richardson, 2012). In view of the fact that lake-level oscillations are documented consistently in the basin, the observed sedimentary sequences are bounded by third-order transgressive events as characterized in the Embry model (Embry, 1993). As such, the studied lake-level variations do not represent depositional sequences as mentioned in the Vail & Mitchum (1977) model, nor genetic stratigraphic sequences as defined by the Galloway (1989) model. Therefore, the local lake-level curve in the present study may be used to analyse the evolution of the Caspian Sea lake-level during the Early Pleistocene.

Caspian Sea lake-level variations seem to have been strongly driven by Early Pleistocene climate conditions. The robust lake-level curve reconstructed in this study includes 20 highstands with an amplitude of *ca* 40 m and a frequency of *ca* 41 kyr. Highstands are in range with the 41 kyr obliquity cycle and correlate in cycle and time domain with obliquity maxima (Fig. 7C). Obliquity minima are known to have strengthened Northern Hemisphere glaciations on the Eurasian continent until the mid-Pleistocene transition (Ruddiman *et al.*, 1989; Maslin *et al.*, 1998). Obliquity minima may have driven increases in

ice-sheets during colder and drier climates in the Caspian catchment areas, which may have caused lake-level lowstands by decreased runoff. Lagoonal and terrestrial settings established around the Kura Basin embayment. On the other hand, obliquity maxima may have generated warmer and wetter climates that drove lake-level highstands by increased northern river runoff. Following lake-level transgressions, the Kura Basin recorded more distal settings mostly driven by regional climate changes.

After the mid-Pleistocene transition, it appears that a strong climatic switch occurred in the Caspian Sea system. Extensive research has shown a correlation between lake-level highstand and glacial conditions (Kroonenberg *et al.*, 1997; Yanina, 2014). Extreme lake-level lowstands likely resulted from water capture in ice-sheets and permafrost during dry periods, whereas lake-level highstands may have resulted from melting of the ice-sheets under humid conditions. Transgression events reached over 150 m amplitude since the Middle Pleistocene, compared to the maximum 40 m amplitude lake-level variations during the Early Pleistocene. The lake-level regime thus experienced a major change during the mid-Pleistocene transition. Overall, Caspian Sea lake-level variations seem to be strongly driven by allogenic forcing mechanisms. Although the present study offers a rare view inside the Early Pleistocene Caspian Sea driven by obliquity climate cycles, further research is still required to fully understand the precise impact and mechanistic pathways of orbital forcing and of (inter)glacial periods on lake-level oscillations.

CONCLUSIONS

During the Early Pleistocene, the Kura Basin formed an embayment of the isolated Caspian Sea. Thick sedimentary successions were deposited on its northern margin, related to high subsidence and aggradation rates. Water and sediment supply originated from northern mountainous sources and from reworked sediment of the Kura Delta confined in the western part of the basin.

The Early Pleistocene Apsheronian regional stage highlights a 1050 m thick interval along the Hajigabul section with eight facies associations representing distal shallow marine to proximal coastal, lagoonal or terrestrial depositional environments. Sediment is deposited in 20 regressive sequences about 60 m thick, bounded by sudden flooding surfaces. The section highlights repeated lake-level changes affecting the Kura Basin embayment.

This geological archive enables reconstruction of a detailed coastal facies model for an isolated sedimentary basin subject to water-level variations. The protected palaeocoastline of the Kura Basin documented limited tide, wind and wave interference, due to reduced storm events compared to the open ocean. This elongated embayment was shielded by the eastern extension of the Greater Caucasus. As a result, the palaeocoastline shaped a low energy, wave-dominated, reflective beach profile. Under these circumstances, wave baselines delimiting the different facies associations (storm-wave base, fair-weather wave base, mean low water level, mean high water level and highest storm level) are assumed to be shallower than in the open ocean.

Frequent lake-level variations occurring along the palaeocoastline of the Kura Basin represent lake-level for the entire Caspian Sea. These are estimated with amplitude of *ca* 40 m water depth and a frequency of *ca* 41 kyr. Lake-level variations in the Early Pleistocene Caspian Sea were possibly driven by the 41 kyr astronomical cycles. This study delivers new insights in terms of coastal morphology along the Caspian Sea, as well as estimations regarding the amplitude, frequency and drivers of relative lake-level changes.

ACKNOWLEDGEMENTS

This research was supported by the project PRIDE (Pontocaspian RIse and DEmise) which has received funding from the European Union's Horizon 2020 research and innovation program, under the Marie Sklodowska-Curie grant agreement No 642973. We are thankful to Jonathan R. Rotzien, Suzanne A.G. Leroy and an anonymous reviewer for their constructive comments that contributed to further improve the manuscript.

REFERENCES

Aagaard, T., **Greenwood, B.** and **Hughes, M.** (2013) Sediment transport on dissipative, intermediate and reflective beaches. *Earth Sci. Rev.*, **124**, 32–50.

Abdullayev, N.R., **Riley, G.W.** and **Bowman, A.P.** (2012) Regional Controls on Lacustrine Sandstone Reservoirs The Pliocene of the South Caspian Basin. In: *Lacustrine Sandstone Reservoirs and Hydrocarbon Systems, Memoir 95* (Eds. O.W. Baganz, Y. Bartov, K. Bohacs and D. Nummedal), pp. 71–98. AAPG, Tulsa.

Abreu, V. and **Nummedal, D.** (2007) Miocene to quarternary sequence stratigraphy of the south and Central Caspian Basins. In: *Oil and Gas of the Greater Caspian area, Studies in Geology*, **55** (Eds. P.O. Yilmaz and G.H. Isaksen), pp. 65–86, AAPG, Tulsa.

Agustí, J., **Vekua, A.**, **Oms, O.**, **Lordkipanidze, D.**, **Bukhsianidze, M.**, **Kiladze, G.** and **Rook, L.** (2009) The Pliocene-Pleistocene succession of Kvabebi (Georgia) and the background to the early human occupation of Southern Caucasus. *Quatern. Sci. Rev.*, **28**, 3275–3280.

Ainsworth, R.B., **Vakarelov, B.K.** and **Nanson, R.A.** (2011) Dynamic spatial and temporal prediction of changes in depositional processes on clastic shorelines: Toward improved subsurface uncertainty reduction and management. *AAPG Bull.*, **95**, 267–297.

Allen, J.R.L. (1963) The classification of cross-stratified units. With notes on their origin. *Sedimentology*, **2**, 93–114.

Allen, M.B., **Vincent, S.J.**, **Alsop, G.I.**, **Ismail-zadeh, A.** and **Flecker, R.** (2003) Late Cenozoic deformation in the South Caspian region: Effects of a rigid basement block within a collision zone. *Tectonophysics*, **366**, 223–239.

Amirinia, G., **Kamranzad, B.** and **Mafi, S.** (2017) Wind and wave energy potential in southern Caspian Sea using uncertainty analysis. *Energy*, **120**, 332–345.

Andrusov, N.I. (1923) Apsheronian Stage. *Proceedings of the Geological Committee 110*, Moscow, 294 pp.

Arpe, K., **Tsuang, B.J.**, **Tseng, Y.H.**, **Liu, X.Y.** and **Leroy, S.A.G.** (2019) Quantification of climatic feedbacks on the Caspian Sea level variability and impacts from the Caspian Sea on the large-scale atmospheric circulation. *Theoret. Appl. Climatol.*, **136**, 475–488.

van Baak, C.G.C., **Vasiliev, I.**, **Stoica, M.**, **Kuiper, K.F.**, **Forte, A.M.**, **Aliyeva, E.** and **Krijgsman, W.** (2013) A magnetostratigraphic time frame for Plio-Pleistocene transgressions in the South Caspian Basin, Azerbaijan. *Global Planet. Change*, **103**, 119–134.

van Baak, C.G.C., **Grothe, A.**, **Richards, K.**, **Stoica, M.**, **Aliyeva, E.**, **Davies, G.R.**, **Kuiper, K.F.** and **Krijgsman, W.** (2019) Flooding of the Caspian Sea at the intensification of Northern Hemisphere Glaciations. *Global Planet. Change*, **174**, 153–163.

Bairamov, A.A., **Aliyev, G.I.**, **Hasanov, G.M.**, **Hasanov, H.Y.**, **Hasanov, T.A.**, **Ismail-Zadeh, A.J.**, **Kangarli, T.N.**, **Korobanov, V.V.**, **Mamedov, A.I.**, **Mamedov, A.V.**, **Mustafayev, H.V.**, **Nagiyev, A.N.**, **Narimanov, A.A.**, **Rustamov, M.I.** and **Zamanov, Y.J.** (2008) Geological map of Azerbaijan Republic. National Academy of Sciences of Azerbaijan Republic, Ministry of Ecology and Natural Resources of Azerbaijan Republic and Ministry of Fuel and Energetics of Azerbaijan Republic, Baku.

Bhattacharya, J.P. and **Giosan, L.** (2003) Wave-influenced deltas: Geomorphological implications for facies reconstruction. *Sedimentology*, **50**, 187–210.

de Boer, P.L., **van Gelder, A.** and **Nio, S.D.** (1988) *Tide-Influenced Sedimentary Environments and Facies*. D. Reidel Publishing Company, Dordrecht, 529 pp.

de Boer, B., **Lourens, L.J.** and **van de Wal, R.S.W.** (2014) Persistent 400,000-year variability of Antarctic ice volume and the carbon cycle is revealed throughout the Plio-Pleistocene. *Nat. Commun.*, **5**, 2999.

Bohacs, K.M., **Carroll, A.R.** and **Neal, J.E.** (2003) Lessons from large lake systems-Thresholds, nonlinearity, and strange attractors. *Geol. Soc. Am. Spec. Pap.*, **270**, 75–90.

Booth, J.G., **Miller, R.L.**, **McKee, B.A.** and **Leathers, R.A.** (2000) Wind induced sediment resuspension in a microtidal estuary. *Cont. Shelf Res.*, **20**, 785–806.

Bourgeois, J. and **Leithold, E.L.** (1984) Wave-worked conglomerates - Depositional processes and criteria for recognition. *Sedimentol. Gravels Conglom.*, **10**, 331–343.

Bouws, E., **Jannink, D.** and **Komen, G.J.** (1996) The increasing wave height in the North Atlantic Ocean. *Bull. Am. Meteor. Soc.*, **77**, 2275–2277.

Caliskan, H. and **Valle-Levinson, A.** (2008) Wind-wave transformations in an elongated bay. *Cont. Shelf Res.*, **28**, 1702–1710.

Campbell, C.V. (1967) Lamina, laminaset, bed and bedset. *Sedimentology*, **8**, 7–26.

Carroll, A.R. and **Bohacs, K.M.** (1999) Stratigraphic classification of ancient lakes: Balancing tectonic and climatic controls. *Geology*, **27**, 99–102.

Catuneanu, O., **Galloway, W.E.**, **Kendall, C.G.S.C.**, **Miall, A.D.**, **Posamentier, H.W.**, **Strasser, A.** and **Tucker, M.E.** (2011) Sequence stratigraphy: methodology and nomenclature. *Newsl. Stratigr.*, **44**, 173–245.

Cheel, R.J. (2006) Horizontal lamination and the sequence of bed phases and stratification under upper-flow-regime conditions. *Sedimentology*, **37**, 517–529.

Chen, J.L., **Wilson, C.R.**, **Tapley, B.D.**, **Save, H.** and **Cretaux, J.F.** (2017) Long-term and seasonal Caspian Sea level change from satellite gravity and altimeter measurements. *J. Geophys. Res.*, **122**, 2274–2290.

Davidson-Arnott, R.G.D. and **van Heyningen, A.G.** (2003) Migration and sedimentology of longshore sandwaves, Long Point, Lake Erie, Canada. *Sedimentology*, **50**, 1123–1137.

Davis, R.A. and **Hayes, M.O.** (1984) What is a wave-dominated coast? *Dev. Sedimentol.*, **39**, 313–329.

Degens, E.T. and **Paluska, A.** (1979) Tectonic and climatic pulses recorded in Quaternary sediments of the Caspian-Black region. *Sed. Geol.*, **23**, 149–163.

Driese, S.G. and **Foreman, J.L.** (1991) Traces and related chemical changes in a Late Ordovician paleosol, Glossifungites ichnofacies, southern Appalachians, USA. *Ichnos*, **1**, 207–219.

Dumas, S. and **Arnott, R.W.C.** (2006) Origin of hummocky and swaley cross-stratification - The controlling influence of unidirectional current strength and aggradation rate. *Geology*, **34**, 1073–1076.

Embry, A.F. (1993) Transgressive–regressive (T–R) sequence analysis of the Jurassic succession of the Sverdrup Basin, Canadian Arctic Archipelago. *Can. J. Earth Sci.*, **30**, 301–320.

Forte, A.M., **Sumner, D.Y.**, **Cowgill, E.**, **Stoica, M.**, **Murtuzayev, I.**, **Kangarli, T.**, **Elashvili, M.**, **Godoladze, T.** and **Javakhishvili, Z.** (2015) Late miocene to pliocene stratigraphy of the kura basin, a subbasin of the south caspian basin: Implications for the diachroneity of stage boundaries. *Basin Res.*, **27**, 247–271.

Frey, S.E. and **Dashtgard, S.E.** (2011) Sedimentology, ichnology and hydrodynamics of strait-margin, sand and gravel beaches and shorefaces: Juan de Fuca Strait, British Columbia, Canada. *Sedimentology*, **58**, 1326–1346.

Galloway, W.E. (1989) Genetic stratigraphic sequences in basin analysis I: Architecture and genesis of flooding-surface bounded depositional units. *AAPG Bull.*, **2**, 125–142.

Grabau, A.W. (1906) Types of sedimentary overlap. *Bull. Geol. Soc. Am.*, **17**, 567–636.

Gradstein, F.M., **Ogg, J.G.**, **Schmitz, M.** and **Ogg, G.** (2012) *The Geologic Time Scale 2012*. Elsevier, Oxford, 1176 pp.

Hamblin, K.W.M. (1961) Micro-cross-lamination in upper Keweenawan sediments of Nothern Michigan. *J. Sediment. Petrol.*, **31**, 390–401.

Hampson, G.J., **Gani, M.R.**, **Sharman, K.E.**, **Irfan, N.** and **Bracken, B.** (2011) Along-Strike and Down-Dip Variations in Shallow-Marine Sequence Stratigraphic Architecture: Upper Cretaceous Star Point Sandstone, Wasatch Plateau, Central Utah, U.S.A. *J. Sediment. Res.*, **81**, 159–184.

Hartgerink, P.E. (2005) *Analysis and Modelling of Wave Spectra on the Caspian Sea*. TU Delft, Delft.

Héquette, A. and **Hill, P.R.** (1993) Storm-generated currents and offshore sediment transport on a sandy shoreface, Tibjak Beach, Canadian Beaufort Sea. *Mar. Geol.*, **113**, 283–304.

Hinds, D.J., **Aliyeva, E.**, **Allen, M.B.**, **Davies, C.E.**, **Kroonenberg, S.B.**, **Simmons, M.D.** and **Vincent, S.J.** (2004) Sedimentation in a discharge dominated fluvial-lacustrine system: The Neogene Productive Series of the South Caspian Basin, Azerbaijan. *Mar. Pet. Geol.*, **21**, 613–638.

Hoogendoorn, R.M., **Boels, J.F.**, **Kroonenberg, S.B.**, **Simmons, M.D.**, **Aliyeva, E.**, **Babazadeh, A.D.** and **Huseynov, D.** (2005) Development of the Kura delta, Azerbaijan; a record of Holocene Caspian sea-level changes. *Mar. Geol.*, **222–223**, 359–380.

Jackson, J., **Priestley, K.**, **Allen, M.** and **Berberian, M.** (2002a) Active tectonics of the South Caspian Basin. *Geophys. J. Int.*, **148**, 214–245.

Jackson, N.L., **Nordstrom, K.F.**, **Eliot, I.** and **Masselink, G.** (2002b) "Low energy" sandy beaches in marine and estuarine environments a review. *Geomorphology*, **48**, 147–162.

Jones, R.W. and **Simmons, M.D.** (1996) A review of the stratigraphy of Eastern Parathethys (Oligocene-Holocene). *Bull. Nat. Hist. Mus. Lond.*, **52**, 25–47.

Jorissen, E.L., **de Leeuw, A.**, **van Baak, C.G.C.**, **Mandic, O.**, **Stoica, M.**, **Abels, H.A.** and **Krijgsman, W.** (2018) Sedimentary architecture and depositional controls of a Pliocene river-dominated delta in the semi-isolated Dacian Basin, Black Sea. *Sed. Geol.*, **368**, 1–23.

Kidwell, S.M. and **Aigner, T.** (1985) Sedimentary dynamics of complex shell beds: implications for ecologic and evolutionary patterns. In: *Sedimentary and Evolutionary Cycles* (Eds U. Bayer and A. Seilacher), pp. 382–395. Springer, Berlin.

Kneale, D. and **Viles, H.A.** (2000) Beach cement: imcipient CaCO3-cemented bearchrock development in the upper intertidal zone, North Uist, Scotland. *Sed. Geol.*, **132**, 165–170.

Kolesnikov, E. (1950) *Paleontology of the USSR*. Academy of Sciences of the USSR, Moscow, pp. 260–288.

Kosarev, A.N. (2005) Physico-geographical conditions of the Caspian Sea. In: *The Handbook of Environmental Chemistry*, Vol. **5** (Ed. O. Hutzinger), pp. 5–31. Springer, Berlin.

Kraus, M.J. and **Hasiotis, S.T.** (2006) Significance of Different Modes of Rhizolith Preservation to Interpreting Paleoenvironmental and Paleohydrologic Settings: Examples from Paleogene Paleosols, Bighorn Basin, Wyoming, U.S.A. *J. Sediment. Res.*, **76**, 633–646.

Krijgsman, W., **Stoica, M.**, **Vasiliev, I.** and **Popov, V.V.** (2010) Rise and fall of the Paratethys Sea during the Messinian Salinity Crisis. *Earth Planet. Sci. Lett.*, **290**, 183–191.

Krijgsman, W., **Tesakov, A.**, **Yanina, T.**, **Lazarev, S.**, **Danukalova, G.**, **Aliyeva, E.**, **Bista, D.**, **Bruch, A.**, **Bukhsianidze, M.**, **Frolov, P.**, **Hoyle, T.M.**, **Jorissen, E.L.**, **Kirscher, U.**, **Koriche, S.A.**, **Kroonenberg, S.B.**, **Lordkipanidze, D.**, **Oms, O.**, **Rausch, L.**, **Singarayer, J.**, **Stoica, M.**, **Titov, V.V.** and **Wesselingh, F.P.** (2019) Quaternary time scales for the Pontocaspian domain : interbasinal connectivity and faunal evolution. *Earth Sci. Rev.*, **188**, 1–40.

Kroonenberg, S.B., **Rusakov, G.V.** and **Svitoch, A.A.** (1997) The wandering of the Volga delta: A response to rapid Caspian sea-level change. *Sed. Geol.*, **107**, 189–209.

Lahijani, H.A.K., **Rahimpour-Bonab, H.**, **Tavakoli, V.** and **Hosseindoost, M.** (2009) Evidence for late Holocene highstands in Central Guilan-East Mazanderan, South Caspian coast, Iran. *Quatern. Int.*, **197**, 55–71.

Lahijani, H.A.K., **Abbasian, H.**, **Naderi Beni, A.**, **Leroy, S.A.G.**, **Haghani, S.**, **Habibi, P.**, **Hosseindust, M.**, **Shahkarami, S.**, **Yeganeh, S.**, **Zandinasab, Z.**, **Tavakoli, V.**, **Vahabi-Asil, F.**, **Azizpour, J.**, **Sayed-Valizadeh, M.**, **Pourkerman, M.** and **Shah-Hosseini, M.** (2019) Sediment distribution pattern of the South Caspian Sea: Possible hydroclimatic implications. *Can. J. Earth Sci.*, **56**, 637–653.

Laskar, J., **Fienga, A.**, **Gastineau, M.** and **Manche, H.** (2011) La2010: A new orbital solution for the long term motion of the Earth. *Astron. Astrophys.*, **532**, 1–15.

Lazarev, S., **Jorissen, E.L.**, **van de, Velde, S.**, **Rausch, L.**, **Stoica, M.**, **Wesselingh, F.P.**, **van, Baak, C.G.C.**, **Yanina, T.A.**, **Aliyeva, E.** and **Krijgsman, W.** (2019) Magneto-biostratigraphic age constraints on the palaeoenvironmental evolution of the South Caspian Basin during the Early-Middle Pleistocene (Kura Basin, Azerbaijan). *Quat. Sci. Rev.*, **222**, 1–26. https://doi.org/10.1016/j.quascirev.2019.105895

Link, M.H. and **Osborne, R.H.** (1978) Lacustrine facies in the Pliocene Ridge Basin Group: Ridge Basin, California. In: *Modern and Ancient Lake Sediments (The International Association of Sedimentologists, Special publications No. 2)* (Eds A. Matter and M.E. Tucker), pp. 167–189. Blackwell Scientific Publications, Oxford.

Mamedov, A.V. (1997) The Late Pleistocene-Holocene history of the Caspian Sea. *Quatern. Int.*, **41**, 161–166.

Martel, A.T. and **Gibling, M.R.** (1991) Wave dominated lacustrine facies and tectonically controlled cyclicity in the lower Carboniferous Horton Bluff Formation, Nova Scotia, Canada. *Spec. Pub. Int. Assoc. Sedimentol.*, **13**, 223–243.

Maslin, M.A., **Li, X.S.**, **Loutre, M.F.** and **Berger, A.** (1998) The contribution of orbital forcing to the progressive intensification of Northern Hemisphere glaciation. *Quatern. Sci. Rev.*, **17**, 411–426.

Matishov, G., **Kovaleva, G.**, **Novenko, E.**, **Krasnorutskaya, K.** and **Pol'shin, V.** (2013) Paleogeography of the Sea of Azov region in the Late Holocene (reconstruction by diatom and pollen data from marine sediments). *Quatern. Int.*, **284**, 123–131.

Medvedev, I.P., **Rabinovich, A.B.** and **Kulikov, E.A.** (2016) Tides in Three Enclosed Basins: The Baltic, Black, and Caspian Seas. *Front. Marine Sci.*, **3**, 1–7.

van der Meulen, F. and **Salman, A.H.P.M.** (1996) Management of Mediterranean coastal dunes. *Ocean Coast. Manag.*, **30**, 177–195.

Miall, A.D. (2006) *The Geology of Fluvial Deposits. Sedimentary Facies, Basin Analysis, and Petroleum Geology*. Springer, Heidelberg, 601 pp.

Morton, A., **Allen, M.**, **Simmons, M.**, **Spathopoulos, F.**, **Still, J.**, **Hinds, D.**, **Ismail-Zadeh, A.** and **Kroonenberg, S.** (2003) Provenance patterns in a neotectonic basin: Pliocene and quaternary sediment supply to the South Caspian. *Basin Res.*, **15**, 321–337.

Nadirov, R.S., **Bagirov, E.**, **Tagiyev, M.** and **Lerche, I.** (1997) Flexural plate subsidence, sedimentation rates, and structural development of the super-deep South Caspian Basin. *Mar. Pet. Geol.*, **14**, 383–400.

Nevesskaja, L.A. (2007) History of the genus Didacna (Bivalvia: Cardiidae). *Paleontological Journal*, **41**, 861–949.

Nichols, G. (2009) *Sedimentology and Stratigraphy*. Wiley-Blackwell, Chichester, 419 pp.

Nielsen, L.H. and **Johannessen, P.N.** (2009) Facies architecture and depositional processes of the Holocene-Recent accretionary forced regressive skagen spit system, Denmark. *Sedimentology*, **56**, 935–968.

Oliveira, C.M.M., **Hodgson, D.M.** and **Flint, S.S.** (2009) Aseismic controls on in situ soft-sediment deformation processes and products in submarine slope deposits of the Karoo Basin, South Africa. *Sedimentology*, **56**, 1201–1225.

Orton, G.J. and **Reading, H.G.** (1993) Variability of deltaic processes in terms of sediment supply, with particular emphasis on grain size. *Sedimentology*, **40**, 475–512.

Otvos, E.G. (2000) Beach ridges - definitions and significance. *Geomorphology*, **32**, 83–108.

Plint, A.G. and **Nummedal, D.** (2000) The falling stage systems tract: recognition and importance in sequence stratigraphic analysis. *Geol. Soc., Lond., Spec. Pub.*, **172**, 1–17.

Popov, S.V., **Shcherba, I.G.**, **Ilyina, L.B.**, **Nevesskaya, L.A.**, **Paramonova, N.P.**, **Khondkarian, S.O.** and **Magyar, I.** (2006) Late Miocene to Pliocene palaeogeography of the Paratethys and its relation to the Mediterranean. *Palaeogeogr. Palaeoclimatol. Palaeoecol.*, **238**, 91–106.

Posamentier, H.W. and **Morris, W.R.** (2000) Aspects of the stratal architecture of forced regressive deposits. *Geol. Soc., Lond., Spec. Pub.*, **172**, 19–46.

Posamentier, H.W., **Jervey, M.T.** and **Vail, P.R.** (1998) Eustatic controls on Clastic Deposition I—Conceptual Framework. *Sea-Level Change.*, **42**, 109–124.

Postma, G. (1990) Depositional architecture and facies of river and fan deltas: a synthesis. *Spec. Pub. Int. Assoc. Sedimentol.*, **10**, 13–27.

Postma, G. (1995) Sea-level-related architectural trends in coarse-grained delta complexes. *Sed. Geol.*, **98**, 3–12.

de Raaf, J.F.M., **Boersma, J.R.** and **van Gelder, A.** (1977) Wave-generated structures and sequences from a shallow marine succession, Lower Carboniferous, County Cork, Ireland. *Sedimentology*, **24**, 451–483.

Reineck, H.E. and **Singh, I.B.** (1972) Genesis of laminated sand and graded rhythmites in storm-sand layers of shelf mud. *Sedimentology*, **18**, 123–128.

Reineck, H.-E. and **Wunderlich, F.** (1968) Classification and origin of flaser and lenticular bedding. *Sedimentology*, **11**, 99–104.

Retallack, G.J. (2001) *Soils of the Past*, 2nd edn. Blackwell Science, Oxford, 404 pp.

Reynolds, A.D., **Simmons, M.D.**, **Bowman, M.B.J.**, **Henton, J.**, **Brayshaw, A.C.**, **Ali-Zade, A.A.**, **Guliyev, I.S.**, **Suleymanova, S.F.**, **Ateava, E.Z.**, **Mamedova, D.N.** and **Koshkarly, R.O.** (1998) Implications of outcrop geology for reservoirs in the neogene productive series: Apsheron Peninsula, Azerbaijan. *AAPG Bull.*, **82**, 25–49.

Richards, K., **van Baak, C.G.C.**, **Athersuch, J.**, **Hoyle, T.M.**, **Stoica, M.**, **Austin, W.E.N.**, **Cage, A.G.**, **Wonders, A.A.H.**, **Marret, F.** and **Pinnington, C.A.** (2018) Palynology and micropalaeontology of the Pliocene - Pleistocene transition in outcrop from the western Caspian Sea, Azerbaijan: Potential links with the Mediterranean, Black Sea and the Arctic Ocean? *Palaeogeogr. Palaeoclimatol. Palaeoecol.*, **511**, 119–143.

Richardson, S.E.J. (2012) *Tectonic, Climatic, and Sedimentary Processes Recorded by Pleistocene Fold Growth Strata, The South Caspian Basin*. Durham University, Azerbaijan.

Ruddiman, W.F., **Raymo, M.E.**, **Martinson, D.G.**, **Clement, B.M.** and **Backman, J.** (1989) Pleistocene evolution: Northern hemisphere ice sheets and North Atlantic Ocean. *Paleoceanography*, **4**, 353–412.

Scarponi, D., **Kaufman, D.**, **Amorosi, A.** and **Kowalewski, M.** (2013) Sequence stratigraphy and the resolution of the fossil record. *Geology*, **41**, 239–242.

Schwartz, R.K. (1982) Bedform and stratification characteristics of some modern small-scale washover sand bodies. *Sedimentology*, **29**, 835–849.

Short, A.D. (2006) Australian beach systems - nature and distribution. *J. Coastal Res.*, **22**, 11–27.

Starek, D., **Pipík, R.** and **Hagarová, I.** (2010) Meiofauna, trace metals, TOC, sedimentology, and oxygen availability in the Late Miocene sublittoral deposits of Lake Pannon. *Facies*, **56**, 369–384.

Stow, D.A.V. and **Tabrez, A.R.** (1998) Hemipelagites: processes, facies and model. *Geol. Soc., Lond., Spec. Pub.*, **129**, 317–337.

Terziev, F.S., **Kosarev, A.N.** and **Kerimova, A.A.** (1992) *Hydrometeorology and Hydrochemistry of the Seas, Part VI, Caspian Sea*. Gidrometeoizdat, Saint Petersbourg, 360 pp.

Vail, P.R. and **Mitchum, R.M.** (1977) Seismic Stratigraphy and Global Changes of Sea Level: Part 1. Overview: Section 2. Application of Seismic Reflection Configuration to Stratigraphic Interpretation. In: *Seismic Stratigraphy - Applications to Hydrocarbon Exploration, Memoir 26* (Ed. C.E. Payton), pp. 51–52. AAPG, Tulsa.

van de Velde, S., **Jorissen, E.L.**, **Neubauer, T.A.**, **Radan, S.**, **Pavel, A.B.**, **Stoica, M.**, **Van Baak, C.G.C.**, **Martínez Gándara, A.**, **Popa, L.**, **de Stigter, H.**, **Abels, H.A.**, **Krijgsman, W.** and **Wesselingh, F.P.** (2019) A conservation palaeobiological approach to assess faunal response of threatened biota under natural and anthropogenic environmental change. *Biogeosciences*, **16**, 2423–2442.

Vespremeanu-Stroe, A., **Zăinescu, F.**, **Preoteasa, L.**, **Tătui, F.**, **Rotaru, S.**, **Morhange, C.**, **Stoica, M.**, **Hanganu, J.**, **Timar-Gabor, A.**, **Cârdan, I.** and **Piotrowska, N.** (2017) Holocene evolution of the Danube delta: An integral reconstruction and a revised chronology. *Mar. Geol.*, **388**, 38–61.

Vincent, S.J., **Davies, C.E.**, **Richards, K.** and **Aliyeva, E.** (2010) Contrasting Pliocene fluvial depositional systems within the rapidly subsiding South Caspian Basin; a case study of the palaeo-Volga and palaeo-Kura river systems in the Surakhany Suite, Upper Productive Series, onshore Azerbaijan. *Mar. Pet. Geol.*, **27**, 2079–2106.

Wesselingh, F.P., **Neubauer, T.A.**, **Anistratenko, V.V.**, **Vinarski, M.V.**, **Yanina, T.**, **Johan, J.**, **Kijashko, P.**, **Albrecht, C.**, **Anistratenko, O.Y.**, **Hont, A.D.**, **Frolov, P.**, **Karpinsky, M.**, **Lattuada, M.**, **Popa, L.**, **Sands, A.F.**, **van de Velde, S.**, **Vandendorpe, J.** and **Wilke, T.** (2019) Mollusc species from the Pontocaspian region – an expert opinion list. *ZooKeys*, **827**, 31–124.

Yanina, T.A. (2014) The Ponto-Caspian region: Environmental consequences of climate change during the Late Pleistocene. *Quatern. Int.*, **345**, 88–99.

Manuscript received 28 May 2019; revision accepted 6 August 2019

Supporting Information

Additional information may be found in the online version of this article:

Appendix S1. Geographic coordinates of the Hajigabul section, with the different logged transects, major faults, remarkable sedimentary layers and regional stages boundaries.
Appendix S2. Detailed sedimentary log of the entire Hajigabul section.
Appendix S3. Faunal assemblages observed along the Hajigabul section with preferred salinities.